POLITECNICO DI MILANO

Facoltà di Ingegneria Industriale

Corso di Laurea Specialistica in
Ingegneria Spaziale

Indirect optimization of time-fixed space transfers with variable specific impulse engine

Relatore: Prof. Franco BERNELLI ZAZZERA
Correlatore: Dr. Pierluigi DI LIZIA

Tesi di Laurea di:

Mirko CATUCCI Matr. 766670

Anno Accademico 2012 - 2013

E quindi uscimmo a riveder le stelle

Dante, *Inferno*

Ringraziamenti

Non è da me parlare tanto, non sono un loquace, ma almeno in questa occasione ci tengo a spendere le giuste parole per le persone meritevoli. Dire grazie mi è sempre stato difficile, non per mancata riconoscenza bensì per introversione. Questa volta avrei piuttosto ritardato il conseguimento della Laurea, ma per nulla al mondo avrei perso l'occasione di ringraziare chi in questi anni mi è stato davvero vicino.

Ringrazio innanzi tutto i miei genitori, che mi hanno dato la vita e che mi hanno permesso di diventare la persona che sono oggi, con anni di duri sacrifici e senza mai avermi fatto pesare l'averli lasciati soli, anche se solo fisicamente, sin dai miei 16 anni. Ho perso molti dei loro compleanni, tantissimi semplici momenti di vita quotidiana e molti altri momenti ugualmente importanti. Sicuramente ne perderò ancora tanti visto che la mia strada è altrove. Dedico soprattutto a loro, quindi, la realizzazione di questo traguardo, la Laurea Specialistica in Ingegneria Spaziale, perché mi hanno dato la possibilità di inseguire i miei sogni, privilegiando la mia felicità alla loro. Gli sono non da meno grato per avermi dato un compagno di viaggio di costante riferimento, mio fratello Davide, e li ringrazio infine per aver forgiato il mio carattere, umile e paziente come mia madre, risoluto e inflessibile come mio padre. Non c'è dottore, ingegnere, contadino o operaio che valga laddove non vi è una persona corretta ed educata.

Un ringraziamento speciale va a nonna Piera, che con non pochi sacrifici mi ha sempre sostenuto. Un pensiero va sicuramente ai nonni che non ci sono più e che non dimenticherò mai. Nonno Remo, che smettendo di fumare e accompagnando me e mio fratello a scuola ha dimostrato di tenere a noi sin da quando siamo nati, e nonna Maria che mi voleva tanto bene e in cui ritrovo tanti aspetti del carattere di mia madre. Un pensiero va infine alla nonnina Angela a cui sono tanto affezionato e al nonno di cui porto il nome e che non ho mai conosciuto. Tante volte mi sono chiesto se sarebbe stato fiero di me se fosse stato ancora in vita e spero con questa Laurea di avergli dato un motivo in più per esserlo.

Subito dopo i nonni, vorrei ringraziare tutti i miei zii, in particolare zia Anna, con cui sin dai primi anni della mia vita ho stretto un legame speciale e che sono contento ci sia oggi nonostante tutte le volte in cui da piccolo (e non solo) le abbia fatto scherzi da infarto. Anche se non intendo farla spaventare ulteriormente, spero di poterle ancora regalare emozioni ugualmente forti ma legate ai traguardi che intendo raggiungere.

Un grazie molto sentito va inoltre a zio Antonio per avermi ospitato durante i miei studi universitari e per essere sempre presente in caso di bisogno.
Un sincero ringraziamento va anche ad alcuni parenti dei miei genitori, che nonostante il lontano grado di parentela mi hanno sempre dimostrato un particolare affetto che naturalmente ricambio: zia Vita e Fernanda.
Infine, ringrazio tutti quei parenti che, nonostante la vita ci abbia allontanato e tolto la possibilità di vederci con maggior frequenza, mi ricordano con piacere e mi portano nel cuore.

Un pensiero non può assolutamente mancare per i compagni di viaggio di questa avventura universitaria, in particolare per quelli che sono e saranno sempre presenti anche fuori dal Politecnico: Elena, una sorella aggiunta (anche se io la chiamo nonna) a cui voglio un bene infinito, Martina, che più di ogni altro è in grado di capirmi ed essermi vicino, Ilaria, grazie a cui ho sorriso dal primo all'ultimo giorno, Brunella, ineguagliabile fonte di ispirazione per battute e scherzi (e che continua a sopportarmi nonostante ciò), Elisa, con cui condivido una rara forma di pazzia, Marco Lucio, che oltre a essere un grande amico mi ha regalato momenti di alta euforia (e follia) ingegneristica, Anna e Luca, sempre presenti e disponibili, e Aniona, con cui ho litigato tante volte ma con cui sono contento di essermi riappacificato (almeno in attesa della prossima lite).

Un ringraziamento anche a due persone che fanno parte di un'avventura precedente, il Liceo, ma che porterò sempre nel cuore: Carlo e Fabio.

Ringrazio tutte le persone che hanno reso indimenticabile il mio Erasmus in Francia, un'esperienza unica nel suo genere che mi ha insegnato ad abbattere tutti i pregidizi xenofobi e a superare sfide di cui non mi ritenevo all'altezza. Merci, donc, de cœur en particulier à David, Alessandra, Rossana, Benjamin, Emilie, Pablo et tous les amis de l'ENSMA et de Poitiers.

Ci tengo inoltre a ringraziare le famiglie di alcuni amici che mi vogliono bene come se facessi parte di loro.
Ringrazio quindi Beatrice e Giovanni, Franco e Cristina, Carmela, Pino e Chiara, Rosaria e Giusy, Franco, Fiorella e Giulia, Luca, Silvia e Nicola, e i genitori di Federico e Oscar che hanno sempre fatto il tifo per me.
Grazie anche a Rosalba e Gianfranco, che dimostrando una sincera amicizia per i miei genitori hanno reso felice anche me.
Ringrazio inoltre gli amici di Saronno, dove mi sono trasferito durante la scrittura della tesi, per avermi accolto tra loro con grande affetto, abbattendo così tutte le difficoltà dovute al trasferimento in una nuova città. A tal proposito ringrazio anche Davide e Lorena per l'ospitalità a Pavia e i genitori

di Alessandra per il loro fondamentale contributo.

Il mio lavoro di tesi è stato svolto con la supervisione del Prof. Bernelli, che ringrazio, e con la guida del mio correlatore, il Dr. Di Lizia, che mi ha seguito da vicino e con cui sono davvero onorato di aver lavorato. Gli sono grato non solo per quello che mi ha trasmesso da un punto di vista tecnico, ma anche umano. Ho sempre pensato all'università come a un luogo in cui ancor prima di imparare le formule scritte sui libri, si venisse stimolati ad apprendere, motivati a superare i propri limiti, un ambiente in cui i propri interessi scientifici venissero continuamente alimentati. Sicuramente Pierluigi rispecchia in pieno questo mio modo di vedere le cose.

Moreover, I am very grateful to Dr. Ranieri. Some passages of my dissertation have been inspired by his PhD work, written in the Univeristy of Texas at Austin in 2007. When I read it, I tried to contact him to ask some questions. Although he has never known me, he has always answered very carefully. Thank you so much Dr. Ranieri for your technical support and your kindness.

Finisco quindi col ringraziare le persone che ho conosciuto durante il periodo della Scuola Militare.
Ringrazio innanzi tutto i Compagni di Corso del Platone II, che mi hanno regalato gli anni più belli della mia vita. Porterò "usque ad inferos" il legame di fratellanza stretto con loro. Mi hanno accettato, sostenuto, voluto bene, dato fiducia e insieme siamo arrivati al traguardo di una gara lunga e faticosa. Grazie anche alle prime persone che hanno creduto in me, il mio Padrino Francesco e il mio Gemello adottivo Antonio. Un abbraccio anche al mio Figlioccio Marco, agli altri Gemellini Domenico, Antonino e Walter e al Nipote Tommaso, che mi hanno dato grandi soddisfazioni e insegnato tanto a loro volta.
Un pensiero a Mattia, per il quale prometto di inseguire i sogni che lui non ha avuto la possibilità di realizzare.
Un ringraziamento inoltre ad alcune tra le persone che considero essere i miei Maestri e da cui ho appreso valori non soltanto appartenenti al mero ambito professionale: la Professoressa Cazzulani, l'allora Capitano Javarone e il Maestro Kurihara.

Ringrazio infine Dio per avermi sempre dato la forza di andare avanti e di mantenere integra la mia onestà intellettuale.

Mirko

Abstract

Space trajectories optimization can be tackled with either direct or indirect methotds. Both need a first guess solution, but indirect methods tend to be more sensitive to the first guess selected. This work aims at mitigating the typical issues related to the application of indirect methods and at defining some general rules, able to keep valid in very heterogeneous mission scenarios. One of the most significant expedients in this direction is the use of polar coordinates, which have shown much more regular trends with respect to Cartesian coordinates.

The work considers time-fixed, low-thrust trajectories and particular attention is payed to variable-specific impulse engines: by varying the amount of energy dedicated to radio frequency heating and the amount of propellant delivered for plasma generation, they are capable of generating either low-thrust, with high–specific impulse exhaust or relatively high-thrust, with low–specific impulse exhaust.

Thanks to optimal control theory, ordinary differential equations for the states and co-states are derived in a minimum-energy problem. Then the attention is focused on the initialization of the co-states. Crucial in this sense were an *Adjoint Control Transformation (ACT)* and the use of a *Polar Curve Fit (PCF)*.

The *ACT* links the initial co-states to some more predictable variables, such as the initial thrust angles. Tipically, the initial co-states are computed more easily in trasfers with a low time of flight. It was observed that, if expressed in polar coordinates, the co-states show an exponential trend as function of the fixed time of flight. So, once the initial co-states of a transfer with a reduced time of flight have been obtained, it is possible through the *PCF* to immediately get the initial co-states for the same transfer but with an increased time of flight.

Once solved the minimum-energy problem, the work addresses the maximization of the final mass. In addition to the previous equations for position and velocity (and their co-states), a mass variation equation appears. Optimal control theory generates a different control law, but the introduction of some helpful assumptions allows to rapidly get a solution for the maximum-final-mass problem.

Then the problem of the saturation of the control is addressed: thrust magnitude is constrained to be lower than an assigned upper bound limit. This is a common but difficult-to-manage problem, as numerical instabilities tipically occur. Nevertheless, a proper combination of *simple* and *multiple shooting techniques* allows to succesfully overcome these problems.

Finally, the performances of the method are assessed on some transfer test

cases, including LEO to LEO, LEO to GEO and Earth to Mars transfers, and a critical analysis of the results is carried out.

The developed method turns out to be effective and robust for all these heterogeneous test cases.

Keywords: Trajectory Optimization, Indirect Methods, Low-Thrust, Optimal Control

Estratto della Tesi

L'ottimizzazione di traiettorie spaziali può avvenire attraverso due principali categorie di metodi: diretti e indiretti. Nei primi è più facile trovare una soluzione di primo tentativo, i secondi permettono di ottenere soluzioni molto più accurate ma richiedono una soluzione di primo tentativo molto vicina a quella ottimale e quindi difficile da trovare. L'obiettivo della tesi è abbattare le difficoltà applicative dei metodi indiretti e definire quindi delle procedure valide in scenari di trasferimento anche molto diversi tra loro. Uno degli accorgimenti più importanti in questo senso è l'uso di coordinate polari: le variabili che definiscono posizione e velocità del satellite hanno dimostrato andamenti molto più regolari se espresse in un sistema di riferimento sferico anziché cartesiano.

Vengono analizzate traiettorie a tempo di trasferimento fissato e a bassa spinta, ovvero facenti uso di propulsione elettrica, la tecnologia più promettente in termini di consumi e flessibilità di impiego. In questa categoria di propulsori, particolare attenzione viene posta verso i motori a impulso specifico variabile, ovvero motori elettromagnetici che, regolando l'energia atta a riscaldare in radio frequenza il propellente e la quantità di gas da destinare alla generazione di plasma, sono capaci di funzionare sia in modalità di alta spinta (e basso impulso specifico) che bassa spinta (e alto impulso specifico).

Tramite le teorie del controllo ottimo vengono dapprima trovate le equazioni differenziali ordinarie di stati e costati che regolano una soluzione di minima energia. Successivamente l'attenzione si concentra sull'inizializzazione dei costati. Fondamentali in questo senso sono la *Adjoint Control Transformation (ACT)* e l'uso di un *Polar Curve Fit (PCF)*.

L'*ACT* definisce delle leggi che legano i costati iniziali con i valori di alcune variabili fisiche più facilmente determinabili, ovvero gli angoli che caratterizzano la direzione del vettore di spinta.

In generale i valori dei costati iniziali sono più facili da trovare in trasferimenti con un ridotto tempo di volo. Si è notato però che molti costati, se espressi in coordinate polari, manifestano un andamento esponenziale in funzione del tempo di trasferimento fissato. Quindi, una volta trovati i costati iniziali di un trasferimento con un basso tempo di volo, è possibile determinare per interpolazione (*PCF*) i costati iniziali di un trasferimento con un tempo di volo sempre più lungo.

Risolto il problema della minimizzazione di energia, viene affrontato quello della massimizzazione della massa finale. In aggiunta alle precedenti equazioni di posizione e velocità (e relativi costati) compare anche l'equazione di variazione della massa. Le teorie del controllo ottimo danno vita a leggi di controllo diverse dal caso precedente, tuttavia l'introduzione di alcune ipotesi

semplificatrici permette di trovare molto rapidamente una prima soluzione al problema di massimizzazione della massa finale.

Successivamente viene affrontato il problema di saturazione del controllo, ovvero lo studio di trasferimenti dove la spinta è vincolata a non superare un valore di soglia prestabilito. Questo è un problema tanto comune quanto di difficile implementazione date le instabilità numeriche che tipicamente insorgono. Ciò nonostante, l'opportuno uso di tecniche di *single* e *multiple shooting* permette di superare con successo tali difficoltà.

A questo punto vengono presi in considerazione alcuni casi studio, quali i trasferimenti tra LEO e LEO, tra LEO e GEO e tra Terra e Marte, e viene presentata un'analisi critica dei risultati.

Il metodo descritto nel corso della tesi si dimostra valido e robusto anche per trasferimenti così eterogenei.

Parole chiave: ottimizzazione di traiettorie, metodi indiretti, bassa spinta, controllo ottimo

Contents

1 Introduction **1**
1.1 State of the Art 1
1.2 Motivation of the work 2
1.3 Proposed Solution 3
1.4 Structure of the dissertation 4

2 Optimal Control Theory **5**
2.1 *Case A*: minimization of thrust acceleration 7
2.1.1 Escape 9
2.1.2 Orbit-to-Orbit transfer 11
2.2 *Case B*: minimization of the propellant consumption 13
2.2.1 Constant Specific Impulse engine 15
2.2.2 Variable Specific Impulse engine 15

3 Numerical techniques, initial guess identification and control saturation **17**
3.1 *Case A*: initial co-states identification 19
3.1.1 Adjoint Control Transformation 19
3.1.2 Polar Curve Fit 22
3.2 *Case A*: complete algorithm 25
3.3 *Case B*: initial co-states identification 29
3.4 *Case B*: optimal control law estimation 32
3.4.1 Control saturation 33
3.5 *Case B*: complete algorithm 34

4 Test Cases **37**
4.1 Common parameters setting 37
4.2 Angles used for the ACT 37
4.3 Code Validation 38
4.4 LEO-to-LEO transfer 43
4.4.1 Solution of Case A 43

4.4.2 Solution of Case B 46
4.4.3 Sensitivity to the maximum thrust 52
4.5 LEO-to-GEO transfer 54
4.5.1 Solution of Case A 54
4.5.2 Solution of Case B 58
4.5.3 Sensitivity to the time of flight 60
4.6 Earth-to-Mars transfer 65

5 Conclusions **71**
5.1 Validity of the Method 71
5.1.1 Flexibility of the method 71
5.1.2 Accuracy of the method 72
5.1.3 Computational efficiency 72
5.2 Future Developments 75

List of Figures

1.1 GTO to Halo orbit by Rasotto 3

2.1 Spherical Reference Frame 6
2.2 125-days Earth escape 10

3.1 Two-Point Boundary Value Problem 18
3.2 Simple Shooting 18
3.3 Multiple Shooting 19
3.4 Vehicle-Centred Reference Frame 20
3.5 *Adjoint Control Transformation* scheme 23
3.6 Optimal $\lambda_{v_{\theta_0}}$ trend 23
3.7 Optimal a_0 trend 24
3.8 Application example of the PCF technique 25
3.9 Algorithm Scheme in the *case A* 28
3.10 Algorithm Scheme in the *case B* 36

4.1 Earth escape: trajectory comparison 39
4.2 Earth escape: acceleration comparison 40
4.3 Earth escape: λ_{r_0} PCF 40
4.4 Earth escape: $\lambda_{v_{r_0}}$ PCF 41
4.5 Earth escape: $\lambda_{v_{\theta_0}}$ PCF 41
4.6 Earth escape: a_0 PCF 41
4.7 Control profile for a thrust-unconstrained LEO-to-LEO transfer 47
4.8 Control profile for a thrust-constrained LEO-to-LEO transfer . 49
4.9 r-profile in a LEO-to-LEO transfer 49
4.10 θ-profile in a LEO-to-LEO transfer 50
4.11 v_r-profile in a LEO-to-LEO transfer 50
4.12 v_θ-profile in a LEO-to-LEO transfer 51
4.13 m-profile in a LEO-to-LEO transfer 51
4.14 LEO-to-LEO transfer 52
4.15 LEO-to-LEO transfer with different T_{max} 53

4.16 PCF for the initial acceleration of a LEO-to-GEO transfer in Case A 55
4.17 Control profile for a thrust-unconstrained LEO-to-GEO transfer 59
4.18 Control profile for a thrust-constrained LEO-to-GEO transfer 60
4.19 LEO-to-GEO, detail of the thrust trend 61
4.20 r-profile in a LEO-to-GEO transfer 61
4.21 θ-profile in a LEO-to-GEO transfer 62
4.22 v_r-profile in a LEO-to-GEO transfer 62
4.23 v_θ-profile in a LEO-to-GEO transfer 63
4.24 m-profile in a LEO-to-GEO transfer 63
4.25 LEO-to-GEO transfer 64
4.26 Thrust-constrained LEO-to-GEO transfer with different TOF 65
4.27 Earth-to-Mars mission, mass 66
4.28 Earth-to-Mars mission, thrust 67
4.29 Earth-to-Mars mission, trajectory 68
4.30 Earth-to-Mars mission, mass 69

List of Tables

4.1 List of relevant constants and coefficients 38

5.1 Performances of the computer used for the implementation of the test cases 73

5.2 Simulation time elapsed to solve the test cases. The Earth-Mars has been analyzed with three different times of flight (TOF), but only the case with $TOF = 350$ *day* is reported in the table, as the simulation time does not significantly change in comparison with the other two cases. 74

Chapter 1

Introduction

Since the Deep Space-1 probe [1] successfully completed its mission much more beyond the best expectations, electric thrusters represent a main propulsion technology for long-duration space missions. Despite the evident benefits that this class of thrusters can generate in terms of cost saving and flexibility, low-thrust trajectory optimization can often result very tricky as it involves the solution of a two-point boundary value problem at least, characterized by a set of non-linear coupled differential equations. This problem can be faced according to different techniques but the most desirable ones in terms of accuracy of the solution are represented by the indirect methods.
The objective of this thesis is to provide a robust algorithm capable of optimizing space trajectories in low-thrust propulsion and in particular the optimiziation is related to the propellant consumption in a time-fixed space transfer.
The work focuses on the use of variable specific impulse engine, as it has been demonstrated [2] that they always guarantee a greater propellant saving with respect to constant specific impulse thrusters.

1.1 State of the Art

The indirect method finds its theoretical foundation in the works of Lawden [3], Bryson and Ho [4], Breakwell [5] and Pontryagin [6], whose *Maximum Principle* represents the master key for space trajectory optimization. Starting from these theoretical basis, lot of researchers tried to perform a space trajectory optimization with low-thrust propulsion, like Petropulos and Russel [7] who studied a minimum-fuel transfer with a circular-restricted-three-body (CR3B) dynamic model, in the Sun-Earth and Jupiter-Europa frames. As they used a constant specific impulse model for the engine, they ended

up with a *bang-bang* control law for the thrust, which has been parametrized with the initial co-states and expressed as a feedback law through the *primer vector theory*. Caillau, Bonnard and Picot [8] focused on an Earth-Moon fuel-optimal transfer in a CR3B model, performing a *continuation* on the mass parameter: the shooting function of an Earth-L2 transfer gives a good approximation of the shooting function of the Earth-Moon transfer. Peng, Zhao, Gao and Wu [9] studied time-fixed transfers between different Halo orbits around the same Lagrangian point exploiting the *invariant stable manifolds theory*. They investigated the possibility of linearizing the optimal control through a *Linear Quadratic Regulation* and compared it with a non-linear optimal control solution. They concluded that, in order to get a fuel-optimal solution, it is indispensable to take into account all the non-linearities because their consideration permits to get appreciable fuel savings. Caillau, Daud and Gergaud [10] formulated a minimum-time solution for CR3B problems by introducing a discrete and a differential homotopy. Thanks to the theory of *conjugate points*, they were able to get second order optimality conditions for the extremals.
Apart from works about Halo-orbit transfers, some authors focused on the indirect optimization of interplanetary trajectories. Casalino and Colasurdo [11] compared the benefits in terms of mass saving when using Constant-Specific-Impulse thrusters, Variable-Specific-Impulse ones or dual-mode thrusters, which operate only at two discrete values of specific impulse. Vadali, Nah and Braden [12] studied a LEO-to-LMO transfer and Ranieri [13] tried to overcome the simplifications they introduced. Mainly, he took into account the gravitational fields of all the three primary attractors (Sun, Earth and Mars) and considered also the phase of *Earth escape* and *Mars capture* that involve spiral trajectories. The techniques Ranieri coinceved for the initialization of the co-states have been greatly exploited in this thesis. Hull [14] studied different mission scenarios and addressed the conversion of optimal control problems into parameter optimization ones.
In the recent years, also *Politecnico di Milano* has focused the attention on space-trajectory indirect optimization. Rasotto [15], formulated a code capable of facing fuel-optimal transfers in two-body and three-body dynamics, including the possibility of performing intermediate fly-by, rendez-vous and gravity assist.

1.2 Motivation of the work

The traditional shortcoming of indirect methods is the difficulty of generating an accurate first guess, which is crucial to ensure convergence. In addition,

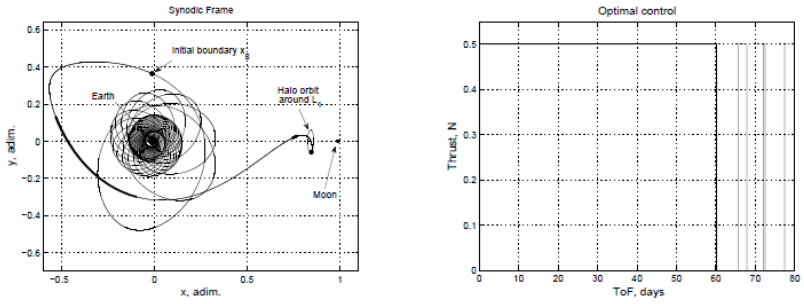

Figure 1.1: Low-thrust transfer from a GTO to an Halo orbit around L1 performed with Rasotto's code. It can be observed that the thrust magntiude was kept constant during the first 60 days.

the more the dynamic equations are non-linear, the more converging to the optimal solution is difficult.

In Rasotto's work [15], non-linearities hindered the method to converge when the spacecraft starting orbit was too close to the primary attractor, so that he could not find the expression of the optimal control law in the first part of the mission. More precisely, during the first 60 days of a GTO-to-Halo-orbit transfer he forced the thrust to be constant in magnitude and alligned to the velocity direction (Figure 1.1).

1.3 Proposed Solution

As a support to Rasotto's work, this thesis tries to reduce the sensitivity to non-linearities, especially for low orbits, by introducing polar coordinates instead of Cartesian ones. It can be tought, indeed, that a more proper choice of the reference frame for the position and velocity variables could help indirect methods to more easily converge to the optimal solution.

Moreover, a variable specific impulse engine is proposed to model the thruster. In this case, the optimization of the propellant consumption produces a continuous control law (Section 2.2.2) instead of "bang-bang" control law that results with a constant specific impulse engine (Section 2.2.1).

As far as the initial guess is concerned, two techniques are used: the *Adjoint Control Transformation (ACT)* and the *Polar Curve Fit (PCF)*. The first one permits to link the initial co-states, which are difficult to estimate, to the thrust angles. The second one helps to find the optimal values for the initial co-states when the time of flight is relatively high thanks to a *continuation* process.

1.4 Structure of the dissertation

Chapter 2 describes the main features of the indirect method and continues with the definition of the dynamic equations expressed in polar coordinates in a *restricted two-body problem*. Then, the attention moves to the optimal control theory and consequently to the derivation of the control law, firstly for a minimum-thrust-acceleration problem (*Case A*), then for a maximum-final-mass problem (*Case B*). Different models for the thrusters are investigated and in particular a *Variable-Specific-Impulse* engine and a *Constant-Specific-Impulse* one.
Chapter 3 describes the techniques adopted to solve the optimal control problem, particularly the *simple shooting* and the *multiple shooting* methods. As far as the *Case A* is concerned, the *Adjoint Control Transformation* and the *Polar Curve Techniques* are exploited to initialize the co-states, whereas for the *Case B* the introduction of a simplifying assumption helps to find an accurate first guess for the initial co-states and the optimal control law in a minimum-propellant-consumption problem. The section concludes explaining how to overcome the numerical difficulties when the control saturation is introduced.
Chapter 4 describes the code validation phase and then the test cases. More specifically, LEO to LEO, LEO to GEO and Earth to Mars are investigated and a critical analysis of the results is performed.
The dissertation ends with Chapter 5, where the validity of the method is discussed and the future developments to be carried are suggested.

Chapter 2

Optimal Control Theory

Optimization problems require the construction of a cost function which includes the quantities to be minimized, as for instance the thrust acceleration or the propellant consumption, and a set of optimality conditions which must be satisfied to ensure optimality. Indirect methods proceed to the differentiation of this cost function through the calculus of variations, ending up with a set of Euler-Lagrange equations which form a boundary value problem. This boundary value problem has an equal number of unknowns and constraints to be fulfilled such as targeted position and velocity conditions. Furthermore, the obtained set of Euler-Lagrange equations includes not only the time variation of the states (position, velocity and mass) but also of the co-states, unphysical variables which mainly help to find the optimal control law, as it is more accurately shown in Sections 2.1 and 2.2. The Euler-Lagrange equations indeed consist in a set of coupled ordinary differential equations where only state and costates appear and, as the order of these ODEs is equal (or can be conducted) to one, only initial conditions are required to solve the problem. As the initial states are generelly known, the main difficulty consists in finding the right initial co-states that guarantee the fulfillment of the constraints. A relevant attention was indeed spent in this direction along the dissertation.

As mentioned before, in order to counteract the effects of the nonlinearities, a spherical reference frame is used. Figure 2.1, taken from [13], shows the difference with a classical $x - y - z$ Cartesian frame. The origin of the system always hosts the primary attractor, x and y axis define its equatorial plane and z completes the right-handed triad. In the spherical sketch, instead, an angle θ spans in the equatorial plane till the projection of r is reached, where r represents the distance of the spacecraft from the primary attractor. Finally, ϕ represents the out-of-plane angle.

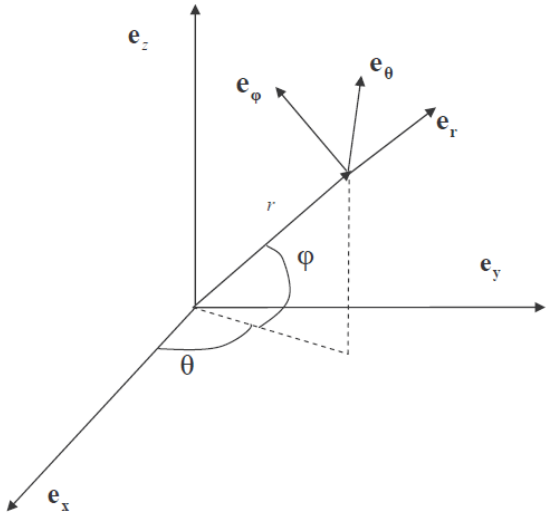

Figure 2.1: Spherical Reference Frame

Altough all the equations will be formulated through polar coordinates, it would not be difficult at all to eventually convert them to the corresponding Cartesian expressions.
When addressing optimal control, the first step consists in describing the dynamics of the system through a state representation which involves only ordinary differential equations of the first order.
Then, it has to be set the cost function J to minimize. In this work, two cases are considered: the minimization of the accumulated thrust acceleration (briefly *case A*) and of the fuel consumption (briefly *case B*). The minimization of the fuel consumption is more commonly investigated, but this first case is easier to menage and helps the definition of the first guess needed by the two-point-boundary-value solvers.
Whatever the selected cost function is, the following relation is always valid,

$$J = G + \int_{t_0}^{t_f} [H - \lambda^T \dot{\mathbf{x}}]\, dt \tag{2.1}$$

where:

- G is the *Boltza function* and collects the portion of the cost function and of the constraints related to a discrete time, for instance the final time;
- H is the *Hamiltonian* and collects the portion of the cost function and of the constraints related to the whole time span.

- λ represents the *co-states*, the unphysical variables introduced to formulate the problem as a boundary value one and to consequently get the expression of the optimal control law.

- $\dot{\mathbf{x}}$ represents the time variation of the *states*.

Observe that this work always treats fixed-time transfers, so t_0 and t_f are known a priori.
As a result of this, the expression of both the Boltza function and of the Hamiltonian are evaluated by the user according to the selected cost function J and the constraints to impose.
Then, by minimizing the cost function with respect to the state and to the control variables, it is possible to end up with the following relations which allow to determine the expression of the co-states time variation and of the optimal controls:

$$\dot{\lambda} = -{H_{\mathbf{x}}}^T \tag{2.2}$$

$$H_{\mathbf{u_c}} = \mathbf{0} \tag{2.3}$$

where $\mathbf{u_c}$ is the vector containing the control variables.

2.1 *Case A*: minimization of thrust acceleration

In this case, the state variables x are the position and velocity variables:

$$\mathbf{x} = \begin{bmatrix} r \\ \theta \\ \phi \\ v_r \\ v_\theta \\ v_\phi \end{bmatrix} \tag{2.4}$$

The dynamic equations will be derived according to a *Restricted Two-Body Problem (RTBP)* model, where only one primary attractor is considered and the second body, the spacecraft, has a mass considerably lower with respect to the first body. The model can be refined by introducing the gravitational effects of other attractors. Exploiting the cardinal law of dynamics, it is possible to define the state variation in time. The reader is referred to [13], pp. 33-34, if interested in the mathematical derivation.

$$\dot{\mathbf{x}} = \begin{bmatrix} v_r \\ v_\theta / r\cos\phi \\ v_\phi / r \\ ({v_\theta}^2 + {v_\phi}^2)/r - \mu/r^2 + a u_r \\ v_\theta(v_\phi \tan\phi - v_r)/r + a u_\theta \\ -(v_r v_\phi + {v_\theta}^2 \tan\phi)/r + a u_\phi \end{bmatrix} \tag{2.5}$$

In the above equations, a represents the thrust acceleration magnitude, whereas u_r, u_θ and u_ϕ are the three components of the unit vector $\mathbf{u}$ which defines the thrust direction. These are actually the control variables included in the vector $\mathbf{u_c}$ and the goal is to determine the expression which minimizes the desired cost function.
Leaving aside for the moment the possible presence of constraints, the Equation 2.1 can be rewritten in this case as

$$\int_{t_0}^{t_f} [-\frac{1}{2}a^2]\, dt = G + \int_{t_0}^{t_f} [H - \lambda^T \dot{\mathbf{x}}]\, dt \tag{2.6}$$

where G is equal to zero and the coefficient $\frac{1}{2}$ has been introduced in order to facilitate the subsequent derivations, without compromising of course the validity of the method.
Rearranging Equation 2.6 it is possible to determine the expression of the Hamiltonian for case A:

$$H = \lambda^T \dot{\mathbf{x}} - \frac{1}{2}a^2 \tag{2.7}$$

Now, it is possible to apply Equations (2.2) and (2.3) in order to get the expressions for $\dot{\lambda}$ and all the compoments of $\mathbf{u_c}$:

$$\begin{bmatrix} \dot{\lambda}_r \\ \\ \dot{\lambda}_\theta \\ \dot{\lambda}_\phi \\ \dot{\lambda}_{v_r} \\ \dot{\lambda}_{v_\theta} \\ \dot{\lambda}_{v_\phi} \end{bmatrix} = \begin{bmatrix} (\lambda_\theta v_\theta + \lambda_\phi v_\phi \cos\phi)/(r^2 \cos\phi) + \lambda_{v_r}[({v_\theta}^2 + {v_\phi}^2)/r^2 - 2\mu/r^3] + \\ \lambda_{v_\theta}(v_\theta v_\phi \tan\phi - v_r v_\theta)/r^2 - \lambda_{v_\phi}(v_r v_\phi + {v_\theta}^2 \tan\phi)/r^2 \\ 0 \\ ({\lambda_{v_\phi}}{v_\theta}^2 - \lambda_{v_\theta} v_\theta v_\phi) 1/\cos^2\phi r - \lambda_\theta v_\theta \tan\phi/(r\cos\phi) \\ -\lambda_r + (\lambda_{v_\theta} v_\theta + \lambda_{v_\phi} v_\phi)/r \\ [\lambda_{v_\theta}(v_r - v_\phi \tan\phi) + 2\lambda_{v_\phi} v_\theta \tan\phi - \lambda_\theta/\cos\phi - 2\lambda_{v_r} v_\theta]/r \\ (\lambda_{v_\phi} v_r - \lambda_\phi - 2\lambda_{v_r} v_\phi - \lambda_{v_\theta} v_\theta \tan\phi)/r \end{bmatrix} \tag{2.8}$$

$$\mathbf{u_c} = \begin{bmatrix} a \\ u_r \\ u_\theta \\ u_\phi \end{bmatrix} = \begin{bmatrix} \lambda_v \\ \lambda_{v_r}/\lambda_v \\ \lambda_{v_\theta}/\lambda_v \\ \lambda_{v_\phi}/\lambda_v \end{bmatrix} \tag{2.9}$$

where λ_v is equal to $\sqrt{\lambda_{v_r}^2 + \lambda_{v_\theta}^2 + \lambda_{v_\phi}^2}$.
Substituting the expressions of the optimal control variables in the 2.4 we get:

$$\dot{\mathbf{x}} = \begin{bmatrix} v_r \\ v_\theta / r\cos\phi \\ v_\phi / r \\ ({v_\theta}^2 + {v_\phi}^2)/r - \mu/r^2 + \lambda_{v_r} \\ v_\theta(v_\phi \tan\phi - v_r)/r + \lambda_{v_\theta} \\ -(v_r v_\phi + {v_\theta}^2 \tan\phi)/r + \lambda_{v_\phi} \end{bmatrix} \tag{2.10}$$

Equations 2.10, togheter with the 2.8, form a set of differential equations of the first order expressed only in function of the states $\mathbf{x}$ and co-states λ. Now, the situation is the one depicted in Figure 3.1 and the next step consists in finding a way to estimate the values of the co-states at the initial time t_0. For this purpuse the *Adjoint Control Transformation (ACT)* is used, which is introduced in Section 3.1.1.

In this work, two kinds of mission are considered: an *escape* and a *orbit-to-orbit transfer* in a Restricted-Two-Body dynamics. In the following sections the attention is focused on how to communicate to the solver the proper constraints to be fulfilled in order to perform the desired kind of mission.

2.1.1 Escape

An escape is a trajectory that targets a fixed level of energy (generally equal to zero) with respect to the primary attractor. In Figure 2.2 it is shown a 125-days Earth escape, targeting a zero-energy condition.

When dealing with constraints in a discrete time, as the final time, the *Bolza Function* G is involved.

In case an escape is performed, G takes the form:

$$G = \rho_{\varepsilon_f}(\varepsilon_f - \varepsilon_{tar}) = \rho_{\varepsilon_f}(\frac{v_f^2}{2} - \frac{\mu}{r_f} - \varepsilon_{tar}) = \rho_{\varepsilon_f}(\frac{v_{r_f}^2 + v_{\theta_f}^2 + v_{\phi_f}^2}{2} - \frac{\mu}{r_f} - \varepsilon_{tar}) \tag{2.11}$$

where ε represents the energy, μ the standard gravitational parameter of the considered main attractor and ρ_{ε_f} the energy multiplier.
Thanks to the optimal control theory, the following relation holds:

$$\lambda_f = G_{\mathbf{x}_f}^T \tag{2.12}$$

In the case of an escape, Equation (2.12) reads:

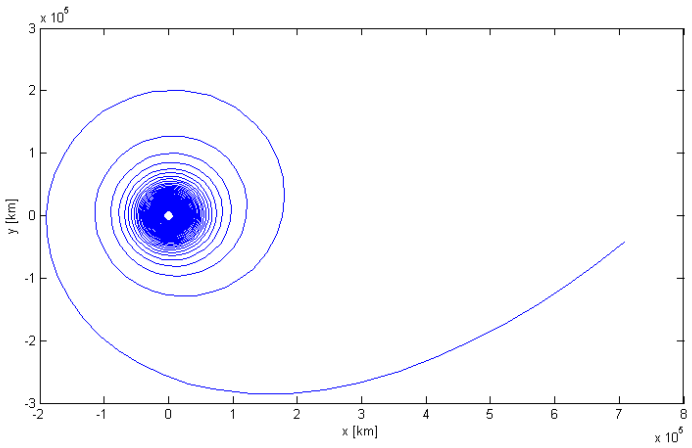

Figure 2.2: 125-days Earth escape

$$\begin{bmatrix} \lambda_{r_f} \\ \lambda_{\theta_f} \\ \lambda_{\phi_f} \\ \lambda_{v_{r_f}} \\ \lambda_{v_{\theta_f}} \\ \lambda_{v_{\phi_f}} \end{bmatrix} = \begin{bmatrix} \rho_{\varepsilon_f}\mu/r_f^2 \\ 0 \\ 0 \\ \rho_{\varepsilon_f} v_{r_f} \\ \rho_{\varepsilon_f} v_{\theta_f} \\ \rho_{\varepsilon_f} v_{\phi_f} \end{bmatrix} \tag{2.13}$$

Observe that as $\dot{\lambda_\theta} = 0$ (Equation 2.8) and $\lambda_{\theta_f} = 0$, λ_θ will be constant and equal to zero along the transfer.

As a result, the number of unknowns matches the number of constraints:

$$\mathbf{z} = \begin{bmatrix} \lambda_{r_0} \\ \lambda_{\phi_0} \\ \lambda_{v_{r_0}} \\ \lambda_{v_{\theta_0}} \\ \lambda_{v_{\phi_0}} \\ \rho_{\varepsilon_f} \end{bmatrix} ; \mathbf{c} = \begin{bmatrix} \varepsilon_f - \varepsilon_{tar} \\ \lambda_{r_f} - \rho_{\varepsilon_f}\mu/r_f^2 \\ \lambda_\phi \\ \lambda_{v_{r_f}} - \rho_{\varepsilon_f} v_{r_f} \\ \lambda_{v_{\theta_f}} - \rho_{\varepsilon_f} v_{\theta_f} \\ \lambda_{v_{\phi_f}} - \rho_{\varepsilon_f} v_{\phi_f} \end{bmatrix} = 0 \tag{2.14}$$

Now, an estimate of $\mathbf{z}$ is required to initialize simple shooting. The question arises spontaneously, that is how to initialize ρ_{ε_f}. The following approach is used in this work: firstly, the ACT is applied to estimate the initial position and velocity co-states. At this point, the complete set of ODEs (2.10) and (2.8) is integrated, so that estimate of λ_{r_f} and r_f is available as well. Finally, the value of ρ_{ε_f} which fulfills the second constraint of Equation (2.14) is computed:

$$\rho_{\varepsilon_f} = \frac{\lambda_{r_f} r_f^2}{\mu} \tag{2.15}$$

2.1.2 Orbit-to-Orbit transfer

An *Orbit-to-Orbit transfer* is a mission that links two fixed orbits. The starting orbit is defined by properly setting the initial position and velocity, while the target orbit is imposed through the Boltza function:

$$\begin{aligned} G = \rho_{r_f}(r_f - r_{tar}) + \rho_{\phi_f}(\phi_f - \phi_{tar}) + \rho_{v_{r_f}}(v_{r_f} - v_{r_{tar}}) + \\ + \rho_{v_{\theta_f}}(v_{\theta_f} - v_{\theta_{tar}}) + \rho_{v_{\phi_f}}(v_{\phi_f} - v_{\phi_{tar}}) \end{aligned} \tag{2.16}$$

Of course the additional term $\rho_{\theta_f}(\theta_f - \theta_{tar})$ must be considered if a particular point on the final orbit is targeted. Again, applying Equation (2.12), it is possible to get an expression for the final co-states:

$$\begin{bmatrix} \lambda_{r_f} \\ \lambda_{\theta_f} \\ \lambda_{\phi_f} \\ \lambda_{v_{r_f}} \\ \lambda_{v_{\theta_f}} \\ \lambda_{v_{\phi_f}} \end{bmatrix} = \begin{bmatrix} \rho_{r_f} \\ 0 \\ \rho_{\phi_f} \\ \rho_{v_{r_f}} \\ \rho_{v_{\theta_f}} \\ \rho_{v_{\phi_f}} \end{bmatrix} \tag{2.17}$$

Keeping the assumption that θ_f is not constrained, it results that $\lambda_\theta = 0$ in all the time domain, being $\dot{\lambda}_\theta$ and λ_{θ_f} equal to zero. Consequently, the unknowns $\mathbf{z}$ and the constraints $\mathbf{c}$ take the following form:

$$\mathbf{z} = \begin{bmatrix} \lambda_{r_0} \\ \lambda_{\phi_0} \\ \lambda_{v_{r_0}} \\ \lambda_{v_{\theta_0}} \\ \lambda_{v_{\phi_0}} \\ \rho_{r_f} \\ \rho_{\phi_f} \\ \rho_{v_{r_f}} \\ \rho_{v_{\theta_f}} \\ \rho_{v_{\phi_f}} \end{bmatrix} ; \mathbf{c} = \begin{bmatrix} r_f - r_{tar} \\ \phi_f - \phi_{tar} \\ v_{r_f} - v_{r_{tar}} \\ v_{\theta_f} - v_{\theta_{tar}} \\ v_{\phi_f} - v_{\phi_{tar}} \\ \lambda_{r_f} - \rho_{r_f} \\ \lambda_{\phi_f} - \rho_{\phi_f} \\ \lambda_{v_{r_f}} - \rho_{v_{r_f}} \\ \lambda_{v_{\theta_f}} - \rho_{v_{\theta_f}} \\ \lambda_{v_{\phi_f}} - \rho_{v_{\phi_f}} \end{bmatrix} = 0 \tag{2.18}$$

Again the problem is how to initialize the multipliers ρ_{r_f}, ρ_{ϕ_f}, $\rho_{v_{r_f}}$, $\rho_{v_{\theta_f}}$ and $\rho_{v_{\phi_f}}$. As for the escape problem, the ACT is used to estimate the position and velocity initial co-states. Then the full set of ODEs (2.10) and (2.8) is integrated to get the approximated values of the final co-states and finally find the "ρ_* multipliers" which fulfill the last constraints $\mathbf{c}$:

$$\begin{bmatrix} \rho_{r_f} \\ \rho_{\phi_f} \\ \rho_{v_{r_f}} \\ \rho_{v_{\theta_f}} \\ \rho_{v_{\phi_f}} \end{bmatrix} = \begin{bmatrix} \lambda_{r_f} \\ \lambda_{\phi_f} \\ \lambda_{v_{r_f}} \\ \lambda_{v_{\theta_f}} \\ \lambda_{v_{\phi_f}} \end{bmatrix} \tag{2.19}$$

The multipliers estimation process presented above already demonstrated to be valid during the test phase. However, an alternative approach has been developed. By carefully studying Equation (2.18) it is evident that the "ρ_* multipliers" do not affect the constraints related to the final states, as it occurred for instance for the escape case, where ρ_{ϵ_f} was multiplied by different position and velocity final states (Equation (2.14)). This means that for the *Orbit-to-Orbit transfer* the "ρ_* multipliers" can be eliminated by the optimization process, so reducing the unknowns and the constraints to:

$$\mathbf{z} = \begin{bmatrix} \lambda_{r_0} \\ \lambda_{\phi_0} \\ \lambda_{v_{r_0}} \\ \lambda_{v_{\theta_0}} \\ \lambda_{v_{\phi_0}} \end{bmatrix}; \mathbf{c} = \begin{bmatrix} r_f - r_{tar} \\ \phi_f - \phi_{tar} \\ v_{r_f} - v_{r_{tar}} \\ v_{\theta_f} - v_{\theta_{tar}} \\ v_{\phi_f} - v_{\phi_{tar}} \end{bmatrix} = 0 \tag{2.20}$$

If these constraints are fulfilled, then the remaining ones will be automatically fulfilled too and the "ρ_* multipliers" will be obtained (if their values are still of interest) for free by equaling them to the respective final co-states:

$$\begin{bmatrix} \rho_{r_f} \\ \rho_{\phi_f} \\ \rho_{v_{r_f}} \\ \rho_{v_{\theta_f}} \\ \rho_{v_{\phi_f}} \end{bmatrix} = \begin{bmatrix} \lambda_{r_f} \\ \lambda_{\phi_f} \\ \lambda_{v_{r_f}} \\ \lambda_{v_{\theta_f}} \\ \lambda_{v_{\phi_f}} \end{bmatrix} \tag{2.21}$$

Of course, if the number of unknowns and constrained is halved, the solver will succeed more easily and rapidly in the optimization process.

2.2 *Case B*: minimization of the propellant consumption

The Case A represents a *minimum-energy solution* and is not able to manage the variation of the spacecraft mass due to the propellant comsumption. Furthermore, it is not so likely that the user is interested in the minimization of the thrust acceleration but rather in the propellant consumption. Despite all this, the Case-A solution permits to get a very accurate initial guess for the Case-B problem, which is in general more difficult to implement. As the matter of facts, one more state variable is involved, the mass, and consequentely another co-state is introduced:

$$\mathbf{x} = \begin{bmatrix} r \\ \theta \\ \phi \\ v_r \\ v_\theta \\ v_\phi \\ m \end{bmatrix} ; \lambda = \begin{bmatrix} \lambda_r \\ \lambda_\theta \\ \lambda_\phi \\ \lambda_{v_r} \\ \lambda_{v_\theta} \\ \lambda_{v_\phi} \\ \lambda_m \end{bmatrix} \tag{2.22}$$

The complete set of state equations is:

$$\dot{\mathbf{x}} = \begin{bmatrix} v_r \\ v_\theta / r\cos\phi \\ v_\phi / r \\ (v_\theta{}^2 + v_\phi{}^2)/r - \mu/r^2 + a u_r \\ v_\theta(v_\phi \tan\phi - v_r)/r + a u_\theta \\ -(v_r v_\phi + v_\theta{}^2 \tan\phi)/r + a u_\phi \\ -T/c \end{bmatrix} \tag{2.23}$$

where T is the thrust and c the *exhaust velocity*, which can be expressed as $2P/T$ or $I_{sp}g$, where P represents the power of the engine, I_{sp} its specific impulse, and g the gravity surface acceleration.

In order to get an expression for the co-state time variation and then for the optimal control law, it is indispensable to write the cost function J and deduce the Hamiltonian H. Observe that, contrary to what happens in Case A, a discrete quantity is optimized in Case B: the final mass m_f (minimizing the fuel consumption is indeed the same as maximizing the final mass of the spacecraft). As a consequence, m_f will belong to the Boltza function G rather than to the Hamiltonian. Referring to Equation (2.1) it follows that $G = m_f$ and $H - \lambda^T \dot{\mathbf{x}} = 0$, so for the Case B the Hamiltonian is equal to:

$$H = \lambda^T \dot{\mathbf{x}} \tag{2.24}$$

At this point, before evaluating the co-states variation and the optimal control law, it is convenient to write the state equations (2.23) in a more compact form, exploiting the vector notation:

$$\begin{bmatrix} \dot{\mathbf{r}} \\ \dot{\mathbf{v}} \\ \dot{m} \end{bmatrix} = \begin{bmatrix} \mathbf{f_r} \\ \mathbf{f_v} + a\mathbf{u} \\ -T/c \end{bmatrix} \tag{2.25}$$

where the vectors $\mathbf{r}$ and $\mathbf{v}$ include respectively the position and velocity variables. So, the Hamiltonian takes the following form:

$$H = \lambda^T \dot{\mathbf{x}} = {\lambda_\mathbf{r}}^T \mathbf{f_r} + {\lambda_\mathbf{v}}^T (\mathbf{f_v} + a\mathbf{u}) + \lambda_m(-T/c) = {\lambda_\mathbf{r}}^T \mathbf{f_r} + {\lambda_\mathbf{v}}^T \mathbf{f_v} + a{\lambda_\mathbf{v}}^T \mathbf{u} - \lambda_m T/c \tag{2.26}$$

Even if the Hamiltonian has a different expression in the Case A and B, it can be easily demonstrated that the optimal control law given by the application of Equation (2.3) yelds again the so-called Lawden's law [3]:

$$\mathbf{u} = \frac{\lambda_\mathbf{v}}{\lambda_v} \tag{2.27}$$

As a consequence, Equation (2.26) can be formulated as:

$$H = {\lambda_\mathbf{r}}^T \mathbf{f_r} + {\lambda_\mathbf{v}}^T \mathbf{f_v} + a\lambda_v - \lambda_m T/c \tag{2.28}$$

where $a = T/m$.

It is now possible to obtain the co-states time variation by applying Equation (2.2):

$$\begin{bmatrix} \dot{\lambda}_r \\ \dot{\lambda}_\theta \\ \dot{\lambda}_\phi \\ \dot{\lambda}_{v_r} \\ \dot{\lambda}_{v_\theta} \\ \dot{\lambda}_{v_\phi} \\ \dot{\lambda}_m \end{bmatrix} = \begin{bmatrix} (\lambda_\theta v_\theta + \lambda_\phi v_\phi \cos\phi)/(r^2 \cos\phi) + \lambda_{v_r}[({v_\theta}^2 + {v_\phi}^2)/r^2 - 2\mu/r^3] + \\ \lambda_{v_\theta}(v_\theta v_\phi \tan\phi - v_r v_\theta)/r^2 - \lambda_{v_\phi}(v_r v_\phi + {v_\theta}^2 \tan\phi)/r^2 \\ 0 \\ ({\lambda_{v_\phi}}{v_\theta}^2 - \lambda_{v_\theta} v_\theta v_\phi)/(r\cos^2\phi) - \lambda_\theta v_\theta \tan\phi/(r\cos\phi) \\ -\lambda_r + (\lambda_{v_\theta} v_\theta + \lambda_{v_\phi} v_\phi)/r \\ [\lambda_{v_\theta}(v_r - v_\phi \tan\phi) + 2\lambda_{v_\phi} v_\theta \tan\phi - \lambda_\theta/\cos\phi - 2\lambda_{v_r} v_\theta]/r \\ (\lambda_{v_\phi} v_r - \lambda_\phi - 2\lambda_{v_r} v_\phi - \lambda_{v_\theta} v_\theta \tan\phi)/r \\ a\lambda_v/m \end{bmatrix} \tag{2.29}$$

Be observed that the expressions for the position and velocity co-states time variation are identical to the Case A.

As far as the optimal control law is concerned, it depends on the selected model for the engine. This work takes into account a *Constant Specific Impulse (CSI)* engine and a *Variable Specific Impulse (VSI)* one [2].

2.2.1 Constant Specific Impulse engine

In the CSI engine the control variables are:

$$\mathbf{u_c} = \begin{bmatrix} \mathbf{u} \\ T \end{bmatrix} \tag{2.30}$$

In order to get the optimal control law, it is convenient to arrange the Hamiltonian expression (2.28) as follows:

$$H = {\lambda_\mathbf{r}}^T \mathbf{f_r} + {\lambda_\mathbf{v}}^T \mathbf{f_v} + S \cdot T \tag{2.31}$$

where S is the *switching function* and is equal to:

$$S = \frac{\lambda_v}{m} - \frac{\lambda_m}{c} \tag{2.32}$$

As mentioned, the Pontryagin maximum principle [6] states that in order to get the optimal control law, the Hamiltonian must be maximized with respect to the control variables (Equation (2.3)). For a CSI engine, this leads to a *bang-bang* control law:

$$T = \begin{cases} T_{max}, & \text{if } S \geq 0 \\ 0, & \text{if } S < 0 \end{cases} \tag{2.33}$$

This law predicts that the thrust can only be null or maximal (from here the name *switching function*), genereting a discontinuous control law. The presence of these discontinuities produces a lot of problems in the implementation phase, so that Rasotto [15] could not perform an optimal control law for orbits close to the primary attractor.

2.2.2 Variable Specific Impulse engine

In the VSI engine there is one more control variable, as the specific impulse can vary to optimize the propellant consumption:

$$\mathbf{u_c} = \begin{bmatrix} \mathbf{u} \\ T \\ P \end{bmatrix} \tag{2.34}$$

In order to get the optimal control law, it is convenient to arrange the Hamiltonian expression (2.28) as follows:

$$H = \lambda_{\mathbf{r}}{}^T \mathbf{f_r} + \lambda_{\mathbf{v}}{}^T \mathbf{f_v} + \frac{T}{m}\lambda_v - \frac{T^2}{2P}\lambda_m \tag{2.35}$$

The application of Equation (2.3) here produces a switch on the power level according to the value of the mass co-state

$$P = \begin{cases} P_{max}, & \text{if } \lambda_m \geq 0 \\ 0, & \text{if } \lambda_m < 0 \end{cases} \tag{2.36}$$

However, the mass co-state time derivative is always positive as can be noted in Equation (3.32) and it will be also shown in Section 3.3 that its initial value can be set as positive. This implies that $\lambda_m \geq 0$ during the whole mission and consequently there will be no switches for a VSI: the power is always kept at its maximal value P_{max} and the control law results to be continuous.

Finally, as far as the thrust is concerned, the application of Equation (2.3) leads also to:

$$T = \lambda_v \frac{P_{max}}{m\lambda_m} \tag{2.37}$$

and consequently:

$$a = \lambda_v \frac{P_{max}}{m^2\lambda_m} \tag{2.38}$$

Substituting this optimal expressions of T and a respectively in the last formulations of $\dot{m}$ and $\dot{\lambda_m}$ (Equation (2.23) and Equation (3.32)), it is obtained that:

$$\dot{m} = -\lambda_v^2 \frac{P_{max}}{2\lambda_m^2 m^2} \tag{2.39}$$

$$\dot{\lambda}_m = \lambda_v^2 \frac{P_{max}}{m^3\lambda_m} \tag{2.40}$$

It is worth observing that in the case of a VSI engine, the resulting thrust is continuous and can be equal not only to zero and T_{max} (as for a CSI engine), but to all the values included in the interval $[0; T_{max}]$.
All the next considerations will be formulated with the assumption that the spacecraft has a VSI engine.

Chapter 3

Numerical techniques, initial guess identification and control saturation

As sketched before, a boundary value problem arises when applying the indirect method. The most common scenario for space-trajectory optimization involves a fixed initial condition for the state variables (position, velocity and mass) and a desired target orbit, which implies conditions on the final values of the position and velocity variables. These final constraints are provided to the solvers as boundary constraints.
In addition, it is requested to find the solution which minimizes the desired cost function. Within the indirect approach to optimal control, this is generally guaranted by expressing the control variables (the thrust magnitude and its direction) as function of the co-states, according to the optimal control theory explained in Chapter 2. Indirect methods do not rely on evaluating the cost function at each iteration, but rather on updating and consequently adjusting the unknowns (states and co-states) according to the current error with respect to the target and optimality conditions.

Consequently, calling $\mathbf{x}$ the state variables and λ the co-states ones, the situation depicted in the Figure 3.1 is usually achieved, where the subscripts 0 and f refer respectively to the initial and the final time, whereas *tar* stays for "targeted condition". As the integration of coupled first order ODEs are is involved in the solution process, the full set of initial conditions to integrate the system is needed. As far as the ODEs integration is concerned, a 4^{th} order variable step Runge-Kutta method was used.

The boundary-value-problem solver aims at determining the values of the unknown initial co-states λ_0 that allow to get the desired final states values $\mathbf{x}_{f_{tar}}$. A *shooting* technique can be used to find λ_0. In the *simple*

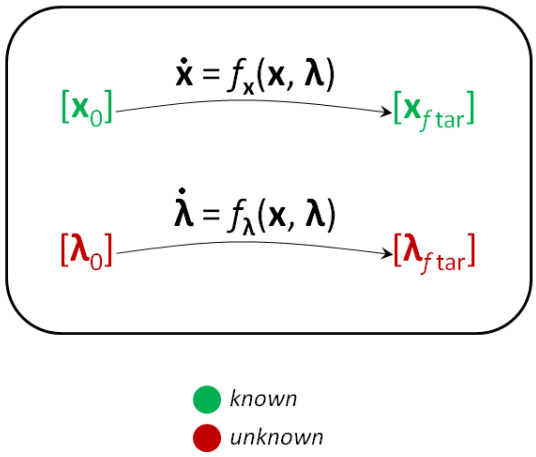

Figure 3.1: Two-Point Boundary Value Problem

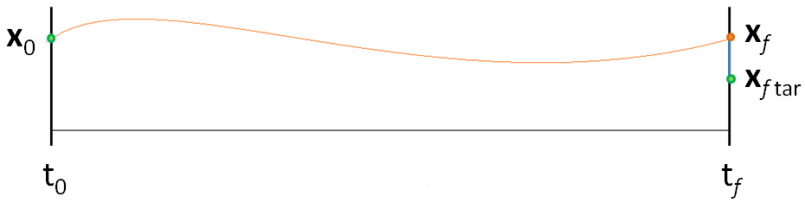

Figure 3.2: Simple Shooting techinque

shooting (Figure 3.2) all the ODEs are integrated till the final time and the difference between the final values of the states ($\mathbf{x}_f$) and the target states ($\mathbf{x}_{f_{tar}}$) is evaluated. If this offset results to be lower than a fixed tollerance, the method has succeeded, otherwise it updates the initial costates and the control using first order corrections.

Unfortunately, the initial co-states that the simple-shooting solver should use as initial guess must be accurate. In order to do this an *Adjoint Control Transformation (ACT)* is performed (Section 3.1.1).

The effectiveness of the simple shooting technique can be increased by dividing the integration time into smaller intervals and, in correspondence of the internal boundaries, by forcing the variables to fulfill continuity constraints. This is the case of the *multiple shooting* technique (Figure 3.3).

With the shooting techniques, the dynamics is so transcribed in a set of equality constraints [18]. As far as the control law is concerned, each time interval is divided into smaller steps through the introduction of internal

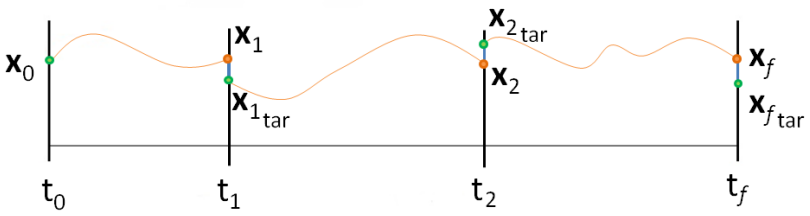

Figure 3.3: Multiple Shooting techinque

nodes. Then the process goes on looking for the node interpolation which allows to propagate the state $\mathbf{x}_i$ to the targeted condition $\mathbf{x}_{(i+1)_{tar}}$.

Multiple shooting is capable of returning more accurate solutions than simple shooting. However, on the other hand, it requires more computational effort: simple shooting solver only needs as input an estimation of the initial co-states, whereas multiple shooting requires a first guess solution in the entire integration time and the definition of the internal targeted conditions.

As a result, a combination of the two techniques was adopted in this work, which turns out to attain the fulfillment of the constraints. It consists of estimating the initial co-states through the ACT, refining them with a *simple shooting* technique, propagating the ODEs with the obtained initial conditions and, finally, using this solution as first guess for the multiple shooting solver.

The presented algorithm enabled the solution of all the test cases shown in Chapter 4.

3.1 *Case A*: initial co-states identification

3.1.1 Adjoint Control Transformation

As sketched before, although the co-states are useful to get the optimal control law, they have no physical meaning and so it is very difficult to predict them. In order to estimate their initial value and enable the solution of the boundary value problem it is crucial to link them to phyisical variables, such as the thrust angles. This is possible thanks to the *Adjoint Control Transformation (ACT)* [16] [17] [2].
The first step consists in introducing the vehicle-centred reference frame shown in Figure 3.4, where the two angles α and γ are used to define the thrust direction. The aim of the *ACT* is to express the co-states as function

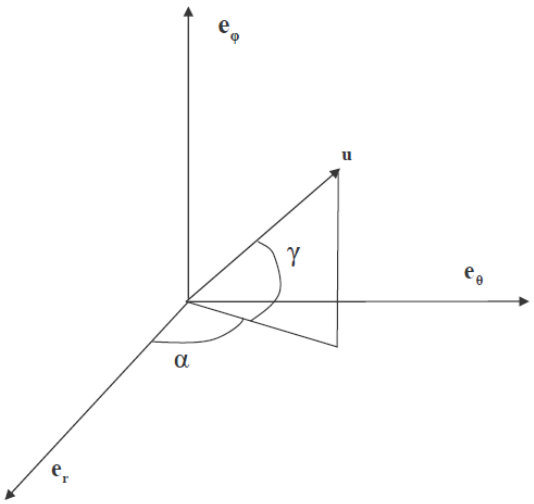

Figure 3.4: Vehicle-Centred Reference Frame

of these angles and their time derivative.

The thrust unit direction vector $\mathbf{u}$ can be forumlated as:

$$\mathbf{u} = \begin{bmatrix} u_r \\ u_\theta \\ u_\phi \end{bmatrix} = \begin{bmatrix} \cos\alpha\cos\gamma \\ \sin\alpha\cos\gamma \\ \sin\gamma \end{bmatrix} \tag{3.1}$$

So, rearranging the last three equations of Equation (2.9) as

$$\lambda_{\mathbf{v}} = \lambda_v \mathbf{u} \tag{3.2}$$

it is possible to write the following relation:

$$\begin{bmatrix} \lambda_{v_r} \\ \lambda_{v_\theta} \\ \lambda_{v_\phi} \end{bmatrix} = \lambda_v \begin{bmatrix} u_r \\ u_\theta \\ u_\phi \end{bmatrix} = \lambda_v \begin{bmatrix} \cos\alpha\cos\gamma \\ \sin\alpha\cos\gamma \\ \sin\gamma \end{bmatrix} \tag{3.3}$$

However, λ_v is equal to the thrust acceleration (see Equation (2.9)). Thus, the velocity co-states can be finally expressed as:

$$\begin{bmatrix} \lambda_{v_r} \\ \lambda_{v_\theta} \\ \lambda_{v_\phi} \end{bmatrix} = a \begin{bmatrix} \cos\alpha\cos\gamma \\ \sin\alpha\cos\gamma \\ \sin\gamma \end{bmatrix} \tag{3.4}$$

This formulation is exploited at the initial time and it shows that, giving an estimation of the initial values of the acceleration a and of the thrust

angles α and γ, it is possible to evaluate the initial velocity co-states.
A similar procedure can be used to derive the position co-states.
Let us start by differentiating Equation (3.2) in time:

$$\dot{\lambda}_{\mathbf{v}} = \dot{\lambda}_v \mathbf{u} + \lambda_v \dot{\mathbf{u}} \tag{3.5}$$

Moving to the scalar notation:

$$\begin{bmatrix} \dot{\lambda}_{v_r} \\ \dot{\lambda}_{v_\theta} \\ \dot{\lambda}_{v_\phi} \end{bmatrix} = \dot{\lambda}_v \begin{bmatrix} u_r \\ u_\theta \\ u_\phi \end{bmatrix} + \lambda_v \begin{bmatrix} \dot{u}_r \\ \dot{u}_\theta \\ \dot{u}_\phi \end{bmatrix} = \dot{\lambda}_v \begin{bmatrix} \cos\alpha\cos\gamma \\ \sin\alpha\cos\gamma \\ \sin\gamma \end{bmatrix} + \lambda_v \begin{bmatrix} -\dot{\alpha}\sin\alpha\cos\gamma - \dot{\gamma}\cos\alpha\sin\gamma \\ \dot{\alpha}\cos\alpha\cos\gamma - \dot{\gamma}\sin\alpha\sin\gamma \\ \dot{\gamma}\cos\gamma \end{bmatrix} \tag{3.6}$$

But, thanks to the optimal control theory, it was already found an expression for $\dot{\lambda}_{v_\theta}$, $\dot{\lambda}_{v_r}$ and $\dot{\lambda}_{v_\phi}$. Taking it from Equation (2.8) and then substituting the expression of λ_{v_θ}, λ_{v_r} and λ_{v_ϕ} stated in Equation (3.3):

$$\begin{bmatrix} \dot{\lambda}_{v_r} \\ \dot{\lambda}_{v_\theta} \\ \dot{\lambda}_{v_\phi} \end{bmatrix} = \begin{bmatrix} -\lambda_r + (\lambda_{v_\theta} v_\theta + \lambda_{v_\phi} v_\phi)/r \\ [\lambda_{v_\theta}(v_r - v_\phi \tan\phi) + 2\lambda_{v_\phi} v_\theta \tan\phi - \lambda_\theta/\cos\phi - 2\lambda_{v_r} v_\theta]/r \\ (\lambda_{v_\phi} v_r - \lambda_\phi - 2\lambda_{v_r} v_\phi - \lambda_{v_\theta} v_\theta \tan\phi)/r \end{bmatrix} =$$

$$\begin{bmatrix} -\lambda_r + \frac{\lambda_v}{r}(\sin\alpha\cos\gamma v_\theta + \sin\gamma v_\phi) \\ -\frac{\lambda_\theta}{r\cos\phi} + \frac{\lambda_v}{r}[\sin\alpha\cos\alpha(v_r - v_\phi\tan\phi) + 2\sin\gamma\tan\phi v_\theta - 2\cos\alpha\cos\gamma v_\theta] \\ -\frac{\lambda_\phi}{r} + \frac{\lambda_v}{r}(\sin\gamma v_r - 2\cos\alpha\cos\alpha v_\phi - \sin\alpha\cos\gamma\tan\phi v_\theta) \end{bmatrix} \tag{3.7}$$

The last operation to perform consists now in matching the second members of Equation (3.6) and Equation (3.7). After a little bit of algebra, it is possible to end up with the following expressions:

$$\lambda_r = \lambda_v[(\sin\alpha\cos\gamma v_\theta + \sin\gamma v_\phi)/r + \dot{\alpha}\sin\alpha\cos\gamma + \dot{\gamma}\cos\alpha\sin\gamma] - \dot{\lambda}_v[\cos\alpha\cos\gamma] \tag{3.8}$$

$$\lambda_\phi = \lambda_v[\sin\gamma v_r - \sin\alpha\cos\gamma\tan\phi v_\theta - 2\cos\alpha\cos\gamma v_\phi - \dot{\gamma}\cos\gamma r] - \dot{\lambda}_v[\sin\gamma] \tag{3.9}$$

$$\dot{\lambda}_v = \lambda_v[\frac{(v_r - v_\phi\tan\phi)}{r} + 2\frac{\tan\gamma\tan\phi}{\sin\alpha}\frac{v_\theta}{r} - 2\cot\alpha\frac{v_\theta}{r} + \dot{\gamma}\tan\gamma - \dot{\alpha}\cot\alpha] +$$

$$-\lambda_\theta[\tfrac{\sec\gamma\sec\phi}{r\sin\alpha}] \tag{3.10}$$

or, remembering that $\lambda_v = a$:

$$\lambda_r = a[(\sin\alpha\cos\gamma v_\theta + \sin\gamma v_\phi)/r + \dot{\alpha}\sin\alpha\cos\gamma + \dot{\gamma}\cos\alpha\sin\gamma] - \dot{\lambda}_v[\cos\alpha\cos\gamma] \tag{3.11}$$

$$\lambda_\phi = a[\sin\gamma v_r - \sin\alpha\cos\gamma\tan\phi v_\theta - 2\cos\alpha\cos\gamma v_\phi - \dot{\gamma}\cos\gamma r] - \dot{\lambda_v}[\sin\gamma] \tag{3.12}$$

$$\dot{\lambda}_v = a[\frac{(v_r - v_\phi\tan\phi)}{r} + 2\frac{\tan\gamma\tan\phi}{\sin\alpha}\frac{v_\theta}{r} - 2\cot\alpha\frac{v_\theta}{r} + \dot{\gamma}\tan\gamma - \dot{\alpha}\cot\alpha] +$$
$$-\lambda_\theta[\tfrac{\sec\gamma\sec\phi}{r\sin\alpha}] \tag{3.13}$$

At this point, particular attention must be payed for λ_θ. It has been demonstrated in Section 2.1.1 that, if the final value of θ is not constrained, then $\lambda_{\theta_f} = 0$. But, as it is known from Equation (2.8), λ_θ keeps constant in time, it is possible to state that also λ_{θ_0} is equal to zero. If so, it is easy to note from Equation (3.13) that $\dot{\lambda}_v$ will be only a function of the initial acceleration, the thrust angles and the initial position and velocity which are assumed to be known. Consequently, the same considerations will hold also for λ_r and λ_ϕ, as can be easily figured out from Equation (3.11) and Equation (3.12).
As far as the physical input variables of the ACT are concerned, it will be shown in Chapter 4.2 how to reasonably initialize them according to the specific mission. Assuming that the final value of θ is not constrained and consequently that λ_θ is always equal to zero, the *Adjoint Control Transformation* can be resumed by Figure 3.5.

Otherwise, an estimate of λ_{θ_0} is required and it cannot be evaluated through the ACT as the number of unknown co-states must be equal to the physical variables introduced.

3.1.2 Polar Curve Fit

Unfortunately, sometimes the estimation of the initial co-states performed through the ACT is not accurate enough to make simple shooting solver converge. This happens mainly when the selected time of flight is very high and, while the thrust angles are relatively easy to estimate, the initial acceleration is not. In this case the regularity of polar coordinates plays a

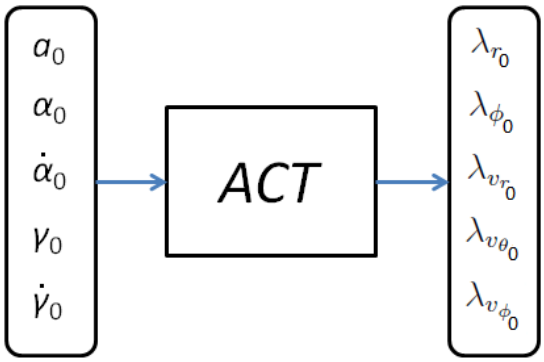

Figure 3.5: *Adjoint Control Transformation* scheme

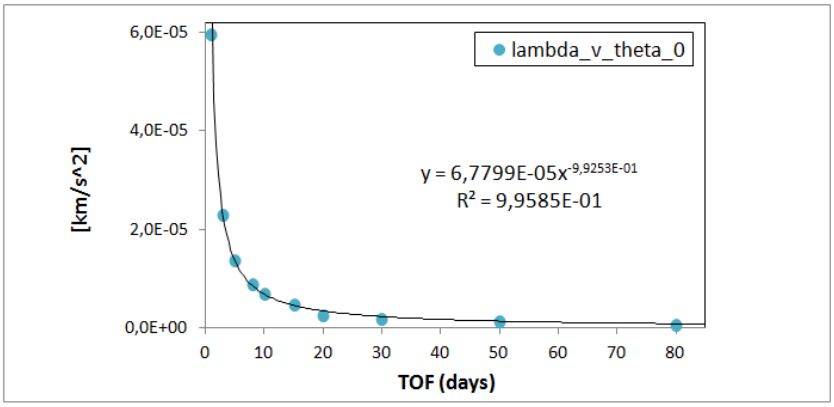

Figure 3.6: Optimal $\lambda_{v_{\theta_0}}$ trend

fundamental role in helping the *simple shooting* technique implementation. In Figure 3.6 it is shown the trend of the values assumed by the optimal $\lambda_{v_{\theta_0}}$ according to the selected time of flight for an Earth-escape trajectory. It can be observed that an exponential-law curve accurately interpolates the experimental optimal co-states represented by the round points. This regular trend can be obtained only through the use of polar coordinates and pertains to most of the co-states, as shown in Chapter 4. But the thrust acceleration is function of the velocity co-states, so if they have a regular trend, the initial acceleration too will follow an exponential curve, as can be noted in Figure 3.7. This is a very good point, because the initial acceleration is the most difficult to be guessed among the parameters required by the *ACT*.

Considering that the lower is the time of flight, the easier are the solver computations, it is strongly recommended to reduce the time of flight if sim-

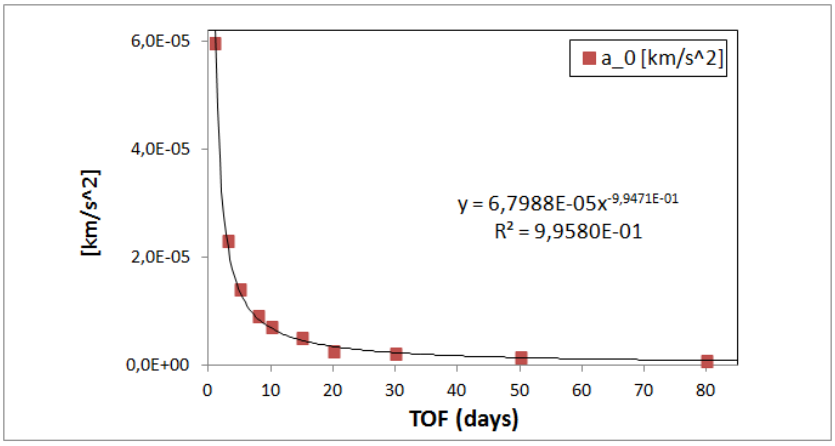

Figure 3.7: Optimal a_0 trend

ple shooting keeps failing. It is highly probable, indeed, that the input a_0 is far from the optimal one. So, it is convenient to start from a lower time of flight, get the optimal a_0 and use it as initial guess for a new integration with a slightly increased time of flight. Thanks to the interpolation process, few values allow to get a good estimate of the optimal initial acceleration for the desired time of flight. Observe that this technique is conceptually identical to a *continuation method*.
A short example is presented to better explain the PCF technique. Imagine one wants to perform an Earth escape in 30 days and that the initial thrust angles are correctly estimated, so only the evaluation of the initial acceleration is missing to exploit the ACT. After lot of attempts, simple shooting keeps failing as the inputed a_0 is highly inaccurate. At this point the user resorts to the PCF techinique and starts to considerably reduce the time of flight, setting it to 3 days for instance. Few attempts allow simple shooting to converge to the optimal a_0 and this value is marked in the graph of Figure 3.8.*a*. Now, the time of flight is slightly increased to 5 days and inputing an accurate a_0 is even easier than before as it is reasonably to imagine that this value will be close to the one found for the 3-day transfer. Once simple shooting finds the optimal initial acceleration for the 5-day escape, it is marked too in the graph of Figure 3.8.*b*. The two optimal a_0 are so interpolated with a polar curve (Figure 3.8.*c*) and this allows to significantly reduce the search space for an accurate guess of the a_0 related to the 30-day escape. If simple shooting still goes in trouble, it is suggested to get other values for the optimal initial acceleration (for instance at 8, 10 and 15 day) before performing the interpolation. The quality of the curve fit will certainly increase and consequently the accuracy of the search space for the 30-day-escape a_0,

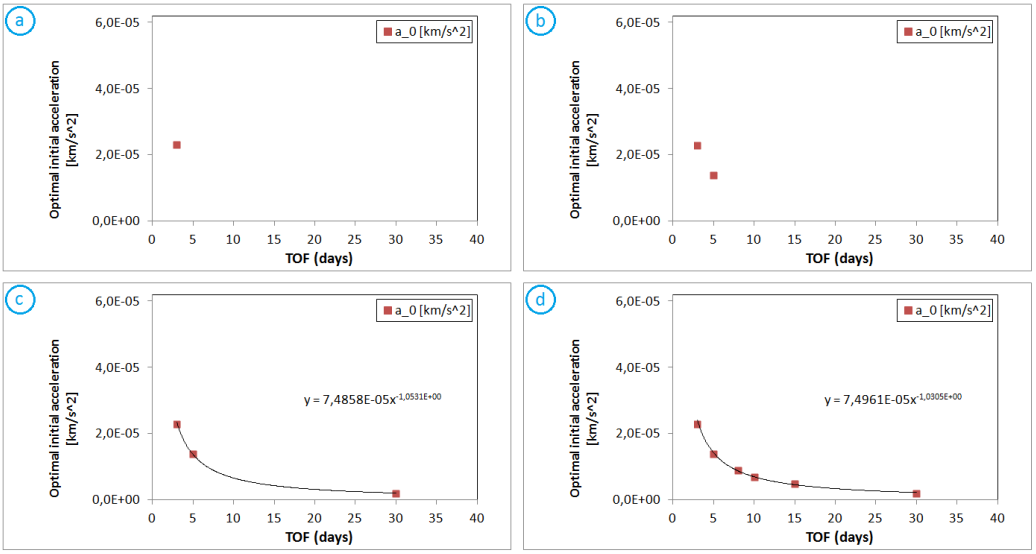

Figure 3.8: Application example of the PCF technique

as shown in Figure 3.8.*d*.

3.2 *Case A*: complete algorithm

Now that all the techniques exploited in Case A have been described, they are collected and resumed in the following algorithm (Figure 3.9):

1. set the aimed time of flight (TOF), the initial state $\mathbf{x}_0$, the tollerance *toll* that the constraints shall not overcome (see Step 5) and the target condition ("*tar*" in Figure 3.9) that consists in the final level of energy ε_{tar} for an escape (Section 2.1.1) and in the final state variables in case of an orbit-to-orbit transfer (Section 2.1.2);

2. define the unknowns $\mathbf{z}$ and the constraints $\mathbf{c}$ according to the selected kind of transfer;

3. estimate:

   (a) the initial thrust angles α_0, $\dot{\alpha}_0$, γ_0 and $\dot{\gamma}_0$;

   (b) the initial acceleration a_0;

4. apply the *simple shooting* technique:

   (a) input a_0, α_0, $\dot{\alpha}_0$, γ_0 and $\dot{\gamma}_0$ to the ACT (Section 3.1.1) in order to get the initial co-state vector λ_0. As the matter of facts, the initial thrust angles and acceleration take the place of the initial co-states in the $\mathbf{z}$ vector; if $\mathbf{z}$ also includes some "ρ_* multipliers", they are estimated thanks to the techniques explained at the end of Section 2.1.1 and 2.1.2 (Equation (2.15) and (2.19));

   (b) now that all the unknowns have been initialized, *simple shooting* can be run. The ODEs (2.10) and (2.8) are integrated starting from $[\mathbf{x}_0,\lambda_0]$;

   (c) simple shooting optimizes the input $\mathbf{z}$ in order to get the optimal $\mathbf{z}_{opt}$ that fulfills the constraints $\mathbf{c}$;

5. once simple shooting finishes to work, the optimized unkwnowns $\mathbf{z}_{opt}$ are obtained and the constraints $\mathbf{c}$ are evaluated. The maximum norm of $\mathbf{c}$, must be lower than the fixed tollerance *toll*. If so, the algorithm jumps to Step 6, otherwise:

   (a) considerably reduce the time of flight;

   (b) proceed with the PCF technique explained in Section 3.1.2;

   (c) obtain a new estimate of the initial acceleration a_0 for the TOF set at Step 1 and repeat the passages from Step 4.a;

6. input the resulting initial thrust angles and acceleration (part of the $\mathbf{z}_{opt}$ vector) to the ACT in order to get the corresponding optimized initial co-states $\lambda_{0_{opt}}$;

7. integrate the ODEs (2.10) and (2.8) starting from $[\mathbf{x}_0,\lambda_{0_{opt}}]$ and get $\mathbf{x}(t)$, $\lambda(t)$;

8. apply the *multiple shooting* technique:

   (a) use the expression of $\mathbf{x}(t)$, $\lambda(t)$ found with the simple shooting as first guess for the multiple shooting;

   (b) define the internal intervals and force state and co-state variables to fulfill continuity conditions;

   (c) run multiple shooting to refine the initial guess solution in order to perfectly fulfill the constraints $\mathbf{c}$;

9. once multiple shooting finishes the optimization process, if all the constraints are equal to zero, then the obtained solution is the optimal one and the algorithm ends; otherwise:

10. reduce the tollerance *toll* and repeat the passages from Step 5.a.

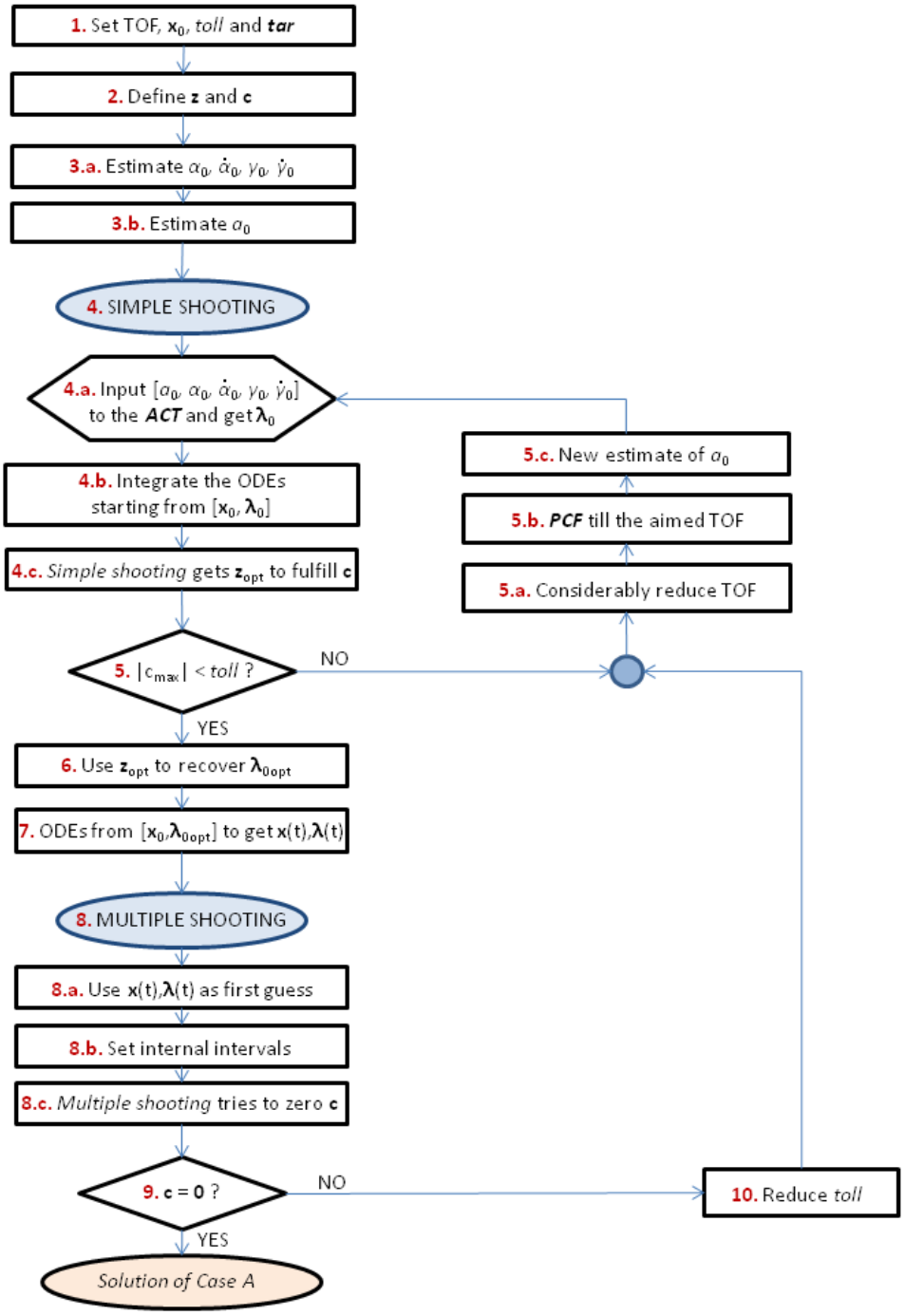

Figure 3.9: Algorithm in *Case A*

3.3 *Case B*: initial co-states identification

As already mentioned, the Case-A solution is exploited as first guess for the Case B, particularly for the initialization of the co-states. At this purpose, the relations that link the two different cases are needed and a method inspired by Ranieri's work [13] is used.

As, similarly to the minimum-energy solution, only position and velocity variables are involved, the Case-A solution lacks of an expression for $\dot{m}$ and $\dot{\lambda}_m$.

The first step consists so in equaling the control law of the two cases:

$$\begin{cases} a_A = a_B \\ \mathbf{u}_A = \mathbf{u}_B \end{cases} \tag{3.14}$$

$$\begin{cases} \lambda_{v_A} = \frac{P_{max}}{m^2 \lambda_m} \lambda_{v_B} \\ \frac{\lambda_{\mathbf{v_A}}}{\lambda_{v_A}} = \frac{\lambda_{\mathbf{v_B}}}{\lambda_{v_B}} \end{cases} \tag{3.15}$$

By solving this very simple system of equations, it results that:

$$\lambda_{v_{r_B}} = \frac{m^2 \lambda_m}{P_{max}} \lambda_{v_{r_A}} \tag{3.16}$$

$$\lambda_{v_{\theta_B}} = \frac{m^2 \lambda_m}{P_{max}} \lambda_{v_{\theta_A}} \tag{3.17}$$

$$\lambda_{v_{\phi_B}} = \frac{m^2 \lambda_m}{P_{max}} \lambda_{v_{\phi_A}} \tag{3.18}$$

and of course:

$$\lambda_{v_B} = \frac{m^2 \lambda_m}{P_{max}} \lambda_{v_A} \tag{3.19}$$

Then, replacing this expression of λ_{v_B} in Equation (2.39):

$$\dot{m} = -\frac{P_{max}}{2\lambda_m^2 m^2} \lambda_{v_B}^2 = -\frac{P_{max}}{2\lambda_m^2 m^2} \frac{m^4 {\lambda_m}^2}{P_{max}^2} \lambda_{v_A}^2 = -\frac{m^2}{2P_{max}} \lambda_{v_A}^2 \tag{3.20}$$

In this way, it is evident that the mass variation is not dependent on λ_m anymore.

Now that the mass and velocity co-states of Case B have been linked to the Case-A solution, only a relation for the position co-states is missing. In order to get it, the first step consists in expressing the ODEs related to position and velocity co-states as function of $\lambda_{\mathbf{B}}$:

$$\begin{bmatrix} \dot{\lambda}_{r_B} \\ \\ \dot{\lambda}_{\theta_B} \\ \dot{\lambda}_{\phi_B} \\ \dot{\lambda}_{v_{r_B}} \\ \dot{\lambda}_{v_{\theta_B}} \\ \dot{\lambda}_{v_{\phi_B}} \end{bmatrix} = \begin{bmatrix} (\lambda_{\theta_B} v_\theta + \lambda_{\phi_B} v_\phi \cos\phi)/(r^2 \cos\phi) + \lambda_{v_{r_B}}[({v_\theta}^2 + {v_\phi}^2)/r^2 - 2\mu/r^3] + \\ \lambda_{v_{\theta_B}}(v_\theta v_\phi \tan\phi - v_r v_\theta)/r^2 - \lambda_{v_{\phi_B}}(v_r v_\phi + {v_\theta}^2 \tan\phi)/r^2 \\ 0 \\ (\lambda_{v_{\phi_B}} {v_\theta}^2 - \lambda_{v_{\theta_B}} v_\theta v_\phi)/(r\cos^2\phi) - \lambda_{\theta_B} v_\theta \tan\phi/(r\cos\phi) \\ -\lambda_{r_B} + (\lambda_{v_{\theta_B}} v_\theta + \lambda_{v_{\phi_B}} v_\phi)/r \\ [\lambda_{v_{\theta_B}}(v_r - v_\phi \tan\phi) + 2\lambda_{v_{\phi_B}} v_\theta \tan\phi - \lambda_{\theta_B}/\cos\phi - 2\lambda_{v_{r_B}} v_\theta]/r \\ (\lambda_{v_{\phi_B}} v_r - \lambda_{\phi_B} - 2\lambda_{v_{r_B}} v_\phi - \lambda_{v_{\theta_B}} v_\theta \tan\phi)/r \end{bmatrix} \tag{3.21}$$

Exploiting Equation (3.16), Equation (3.17) and Equation (3.18), it can be easily demonstrated that

$$\dot{\lambda}_{r_B} = \frac{m^2 \lambda_m}{P_{max}} \dot{\lambda}_{r_A} \tag{3.22}$$

$$\dot{\lambda}_{\theta_B} = \frac{m^2 \lambda_m}{P_{max}} \dot{\lambda}_{\theta_A} \tag{3.23}$$

$$\dot{\lambda}_{\phi_B} = \frac{m^2 \lambda_m}{P_{max}} \dot{\lambda}_{\phi_A} \tag{3.24}$$

and consequently:

$$\lambda_{r_B} = \frac{m^2 \lambda_m}{P_{max}} \lambda_{r_A} \tag{3.25}$$

$$\lambda_{\theta_B} = \frac{m^2 \lambda_m}{P_{max}} \lambda_{\theta_A} \tag{3.26}$$

$$\lambda_{\phi_B} = \frac{m^2 \lambda_m}{P_{max}} \lambda_{\phi_A} \tag{3.27}$$

At this point, in order to get the initial co-states, Equations (3.25)-(3.27) and Equations (3.16)-(3.18) are evaluated at the initial time. So, for the position and velocity co-states, it results that:

$$\lambda_{\mathbf{v},\mathbf{r_{B_0}}} = \frac{m_0^2 \lambda_{m_0}}{P_{max}} \lambda_{\mathbf{v},\mathbf{r_{A_0}}} \tag{3.28}$$

As far as λ_{m_0} is concerned, it can be set to any positive value, as it has been shown in Equation (3.20) that under the presented assumptions its value does not affect the states but just scales the co-states values.
It is worth observing that in Case B, G is equal to the Bolza function of Case A (Equation (2.11) for the *escape* and Equation (2.11) for the *orbit-to-orbit transfer*) increased by the term m_f:

$$G_B = G_A + m_f \tag{3.29}$$

Thus, when applying Equation (2.12), one more constraint with respect to Case A arises:

$$\mathbf{c}_B = \begin{bmatrix} \mathbf{c}_A \\ \lambda_{m_f} - 1 \end{bmatrix} = \mathbf{0} \tag{3.30}$$

Imagine now that the initial mass multiplier λ_{m_0} is set to one. As the mass co-state increases in time, after the ODEs integration λ_{m_f} will be equal to a positive constant K greater than one. One could think that setting $\lambda_{m_0} = 1$ is wrong, but actually this choice only scales the co-states and does not affect the optimization process: in such a way the optimized cost function J will be equal to Km_f. As K is a constant, optimizing Km_f is in practical terms the same as optimizing m_f. So, again, setting λ_{m_0} equal to one is correct and allows the fulfillment of all the Case-B constraints [2].

Now that all the initial co-states are known, the full set of the following states and co-states ODEs can be integrated:

$$\begin{bmatrix} \dot{r} \\ \dot{\theta} \\ \dot{\phi} \\ \dot{v_r} \\ \dot{v_\theta} \\ \dot{v_\phi} \\ \dot{m} \end{bmatrix} = \begin{bmatrix} v_r \\ v_\theta / r \cos\phi \\ v_\phi / r \\ ({v_\theta}^2 + {v_\phi}^2)/r - \mu/r^2 + \lambda_{v_{r_B}} P_{max}/(\lambda_m m^2) \\ v_\theta(v_\phi \tan\phi - v_r)/r + \lambda_{v_{\theta_B}} P_{max}/(\lambda_m m^2) \\ -(v_r v_\phi + {v_\theta}^2 \tan\phi)/r + \lambda_{v_{\phi_B}} P_{max}/(\lambda_m m^2) \\ -\lambda_{v_B}^2 P_{max}/(2\lambda_m^2 m^2) \end{bmatrix} \tag{3.31}$$

$$\begin{bmatrix} \dot{\lambda}_{r_B} \\ \dot{\lambda}_{\theta_B} \\ \dot{\lambda}_{\phi_B} \\ \dot{\lambda}_{v_{r_B}} \\ \dot{\lambda}_{v_{\theta_B}} \\ \dot{\lambda}_{v_{\phi_B}} \\ \dot{\lambda}_m \end{bmatrix} = \begin{bmatrix} (\lambda_{\theta_B} v_\theta + \lambda_{\phi_B} v_\phi \cos\phi)/(r^2 \cos\phi) + \lambda_{v_{r_B}}[(v_\theta{}^2 + v_\phi{}^2)/r^2 - 2\mu/r^3] + \\ \lambda_{v_{\theta_B}}(v_\theta v_\phi \tan\phi - v_r v_\theta)/r^2 - \lambda_{v_{\phi_B}}(v_r v_\phi + v_\theta{}^2 \tan\phi)/r^2 \\ 0 \\ (\lambda_{v_{\phi_B}} v_\theta{}^2 - \lambda_{v_{\theta_B}} v_\theta v_\phi)/(r\cos^2\phi) - \lambda_{\theta_B} v_\theta \tan\phi/(r\cos\phi) \\ -\lambda_{r_B} + (\lambda_{v_{\theta_B}} v_\theta + \lambda_{v_{\phi_B}} v_\phi)/r \\ [\lambda_{v_{\theta_B}}(v_r - v_\phi \tan\phi) + 2\lambda_{v_{\phi_B}} v_\theta \tan\phi - \lambda_{\theta_B}/\cos\phi - 2\lambda_{v_{r_B}} v_\theta]/r \\ (\lambda_{v_{\phi_B}} v_r - \lambda_{\phi_B} - 2\lambda_{v_{r_B}} v_\phi - \lambda_{v_{\theta_B}} v_\theta \tan\phi)/r \\ \lambda_{v_B}^2 P_{max}/(\lambda_m m^3) \end{bmatrix} \tag{3.32}$$

Observe that, thanks to Equation (3.28), once the Case A is solved, one only needs to set the initial mass of the spacecraft m_0 and the engine maximal power P_{max} to immediately get the solution for the "unconstrained"-Case-B problem, that is the case in which any control saturation is imposed. From now on, the "constrained" solution will instead refer to a solution that inculdes a control saturation.

3.4 *Case B*: optimal control law estimation

It is worth observing that, in order to obtain an unconstrained-Case-B solution, there is no need at all to estimate the co-states, as, exploting the previous assumptions and relations, the state equations can be written in the following form:

$$\dot{\mathbf{x}} = \begin{bmatrix} v_r \\ v_\theta/r\cos\phi \\ v_\phi/r \\ (v_\theta{}^2 + v_\phi{}^2)/r - \mu/r^2 + \lambda_{v_{r_A}} \\ v_\theta(v_\phi \tan\phi - v_r)/r + \lambda_{v_{\theta_A}} \\ -(v_r v_\phi + v_\theta{}^2 \tan\phi)/r + \lambda_{v_{\phi_A}} \\ -m^2 \lambda_{v_A}^2/(2P_{max}) \end{bmatrix} \tag{3.33}$$

If instead a constrained solution is of interest, all the $\lambda_{\mathbf{B}}$ must be taken into account, making so their ODEs integration and consequently the estimation of their initial values necessary, as shown in Section 3.3. Moreover, in order to compute the constrained solution, the unconstrained one is inputed to the solver as first guess.

3.4.1 Control saturation

In the followings, the procedure to set an upper limit to the thrust is presented. Observe that the same method can be applied with very slight and intuitive modifications to impose a lower limit to the thrust, bounds on the specific impulse or on the acceleration.
A sort of decoupling between the states and the co-states variables is performed. Indeed, in the state ODEs, the co-states do not appear anymore and the control is expressed as function of the thrust:

$$\begin{bmatrix} \dot{r} \\ \dot{\theta} \\ \dot{\phi} \\ \dot{v_r} \\ \dot{v_\theta} \\ \dot{v_\phi} \\ \dot{m} \end{bmatrix} = \begin{bmatrix} v_r \\ v_\theta / r \cos\phi \\ v_\phi / r \\ ({v_\theta}^2 + {v_\phi}^2)/r - \mu/r^2 + T_r/m \\ v_\theta(v_\phi \tan\phi - v_r)/r + T_\theta/m \\ -(v_r v_\phi + {v_\theta}^2 \tan\phi)/r + T_\phi/m \\ -T^2/2P_{max} \end{bmatrix} \tag{3.34}$$

At this point both the state and the co-states ODEs are integrated but at each time step the following algorithm must be performed.

Firstly, the thrust components are set to:

$$T_r = \frac{\lambda_{v_r} P_{max}}{\lambda_m m} \tag{3.35}$$

$$T_\theta = \frac{\lambda_{v_\theta} P_{max}}{\lambda_m m} \tag{3.36}$$

$$T_\phi = \frac{\lambda_{v_\phi} P_{max}}{\lambda_m m} \tag{3.37}$$

Then the current value of the thrust is computed:

$$T = \sqrt{T_r^2 + T_\theta^2 + T_\phi^2} \tag{3.38}$$

Finally, if $T \geq T_{max}$ the thrust components are re-scaled:

$$T_r = \frac{T_{max}}{T} T_r \tag{3.39}$$

$$T_\theta = \frac{T_{max}}{T} T_\theta \tag{3.40}$$

$$T_\phi = \frac{T_{max}}{T} T_\phi \tag{3.41}$$

and then the full state of ODEs is ready for the integration in the next time step.

3.5 *Case B*: complete algorithm

Now that all the techniques exploited in Case B have been described, they are collected and resumed in the following algorithm (Figure 3.10):

1. set the initial mass m_0 and the maximum power level P_{max} achievable by the engine;
2. assume that the control laws for Case A and B are the same (Equation (3.15));
3. thanks to this assumption:
   (a) set $\lambda_{m_0} = 1$, as its value does not affect the states and control profiles but only scales the co-states (see Equation (3.20));
   (b) recover an expression for the initial position and velocity co-states $\lambda_{\mathbf{B_{v,r_0}}}$ once the optimal $\lambda_{\mathbf{A_{v,r_0}}}$ are known (Equation (3.28));
4. integrate the ODEs (3.31) and (3.32) starting from $\mathbf{x}_0$ and $\lambda_{\mathbf{B_0}}$, with $\lambda_{\mathbf{B}0} = [\lambda_{\mathbf{B_{v,r_0}}}; \lambda_{m_0}]$. As a result, the "*unconstrained*" solution is obtained, that is the solution of Case B with any imposed control saturation;
5. in order to get a "*constrained*" solution, start setting the maximum achievable thrust T_{max};
6. apply multiple shooting techinique remarking that:
   (a) the state ODEs must be decoupled from the co-states, expressing them as function of the control variables (Equations (3.34));
   (b) the transformations described by Equations (3.35), (3.36) and (3.37) must be performed at each time step, computing so the current value of the thrust (Equation (3.38));
7. if the current thrust is greater than the fixed T_{max}, then:
   (a) re-scale the thrust components according to Equations (3.39), (3.40) and (3.41);

otherwise skip Step 7.a and go directly to Step 8:

8. integrate the full set of ODEs (3.31) and (3.32) till the subsequent time step and repeat passages from Step 6.b till the final time is reached; then:

9. if multiple shooting successfully converges, the obtained solution is the optimal *constrained* one, otherwise:

10. augment T_{max} and repeat passages from Step 6.

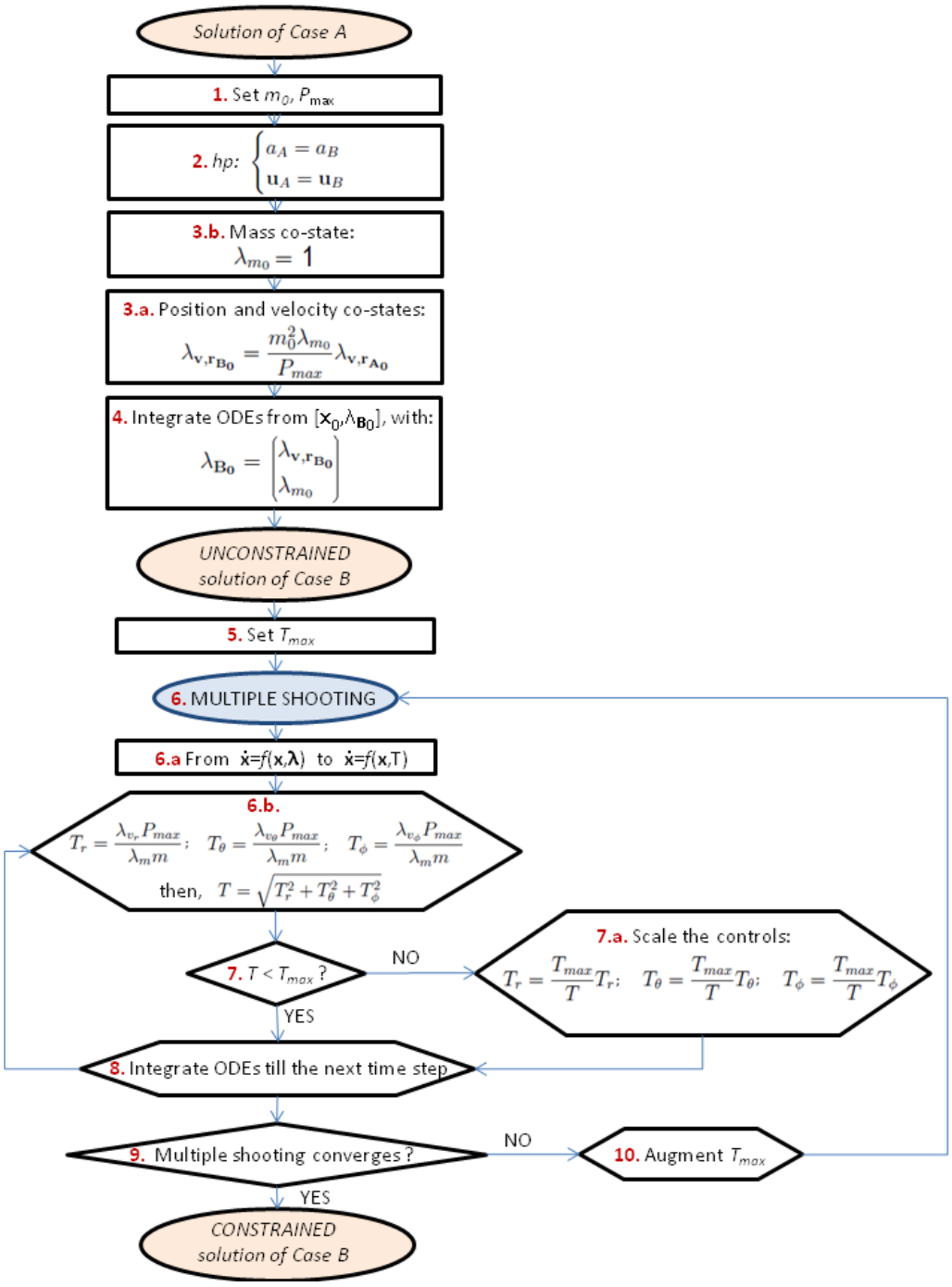

Figure 3.10: Algorithm in *Case B*

Chapter 4

Test Cases

This Chapter presents and critically discusses the analyzed test cases, which are the Earth escape, the LEO-to-LEO, the LEO-to-GEO and the Earth-to-Mars transfers (respectevely Section 4.3, Section 4.4, Section 4.5 and Section 4.6). Before addressing test cases, the parameters used for the astronomical quantities and the Adjoint Control Transformation are reported in Section 4.1 and Section 4.2, respectively.

4.1 Common parameters setting

For the sake of completeness and to allow other researchers to reproduce the results shown in this thesis, Table 4.1 reports the most relevant constants and coefficients used by the author during the computation phase.

4.2 Angles used for the ACT

The angles inputed as first guess to the Adjoint Control Transformation are here shown and discussed. In the presented missions the trajecory is always planar as both the starting and target orbits lie on the same plane. This means that the out-of-plane angle γ (see Figure 3.5) is always equal to zero, as well as its time derivative $\dot{\gamma}$. As far as the initial value of the in-plane angle α is concerned, in all the test cases the starting orbit is circular. Thus the velocity is initially tangential and so aligned with the $\mathbf{e}_\theta$ unit vector. It is assumed that the thrust is aligned with the velocity vector at the initial time t_0. As a result, α_0 can be considered equal to $\pi/2$. In addition, its time derivative $\dot{\alpha}_0$ can be initialized to zero, imagining that the thrusters do not significaly change their direction in the first seconds of the mission.

Symbol	Description	Value
μ_{Earth}	Gravitational Parameter of the Earth	$3.986 \cdot 10^5 km^3/s^2$
μ_{Sun}	Gravitational Parameter of the Sun	$1.32712440018 \cdot 10^{11} km^3/s^2$
g_{Earth}	Gravity Surface Acceleration of the Earth	$9.81 \cdot 10^{-3} km/s^2$
g_{Sun}	Gravity Surface Acceleration of the Sun	$274.0 \cdot 10^{-3} km/s^2$
AU	Astronomical Unit	$149.6 \cdot 10^6 km$
$d_{Sun-Earth}$	Sun-Earth distance	$1AU$
$d_{Sun-Mars}$	Sun-Mars distance	$1.52AU$

Table 4.1: List of relevant constants and coefficients

The presented values represent a first guess for the optimal thrust angles, which are subsequently optimized thanks to simple shooting.

4.3 Code Validation

As stated in Chapter 1, Ranieri's work [13] is the main reference for this thesis. He treated an Earth-Mars optimal transfer with low-thrust propulsion and divided the integration of the trajectory in three distinct phases: the Earth escape, the Eliocentric leg and the Mars capture. Earth escape is intended to be a transfer which starts from a LEO and targets a condition of zero energy with respect to the Earth, whereas the "capture" represents exactly the opposite: starting from a condition of zero energy with respect to Mars, the spacecraft has to reach a fixed LMO (Low Mars Orbit). In both the first and the last phase, a spiral trajectory is obtained and Ranieri noted that, for such kind of trajectory, a polar coordinate frame considerably reduces the numerical difficulties. He showed indeed the regularity trend of the co-states with respect to the fixed time of flight, so that it was possible to apply a *Polar Curve Fit (PCF)* to quickly estimate them. This work investigates if the regularity of the polar coordinates and the *PCF* remain valid for other kinds of transfers, mainly between two circular orbits around the same primary attractor. As a first step, the approach developed in this

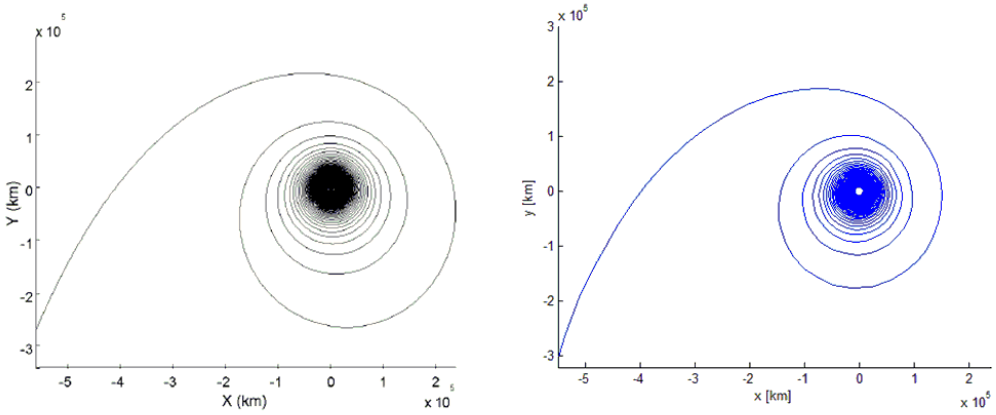

Figure 4.1: Earth escape: trajectory comparison between Ranieri's result *(left)* and Catucci's one *(right)*

work is validated against one of the results obtained by Ranieri. A 150-days Earth escape is chosen as test case, starting from a circular orbit with a semi-major axis equal to 7500km.

In Figure 4.1 the trajectory obtained by Ranieri and the author are shown. It can be easily observed that the two trajectories are very similar. The small difference can be related to the fact that Ranieri does not report the true anomaly of the starting point on the LEO. So a different initial condition might have been selected in this work. Despite this, the obtained result has been considered satisfactory.

In Figure 4.2 the acceleration profiles obtained by Ranieri and the author are compared. As can be seen, the control profiles are very similar.

In addition, as the selected time of flight is relatively high, a polar curve fit was performed. Figure 4.3 - 4.6 show the obtained results for the PCF and compare them with Ranieri's ones. The parameter called R^2 describes the accuracy of the interpolation: the more R^2 is close to one, the more the curve fit is accurate. Although the PCF has been performed till a time of flight equal to 150 days, for the sake of clarity the graphs have been zoomed showing a reduced x-axis. Despite some slight difference for the numerical values, the trends are qualitatively identical. Only $\lambda_{v_{r_0}}$ shows a more significant difference but, as Ranieri himself highlights, it is the most irregular co-state.

All the presented results allow to consider the code successfully validated.

Observe that λ_ϕ and λ_{v_ϕ} are not shown because the considered transfer is planar and more precisely it occurs in the equatorial plane, so the out-of-

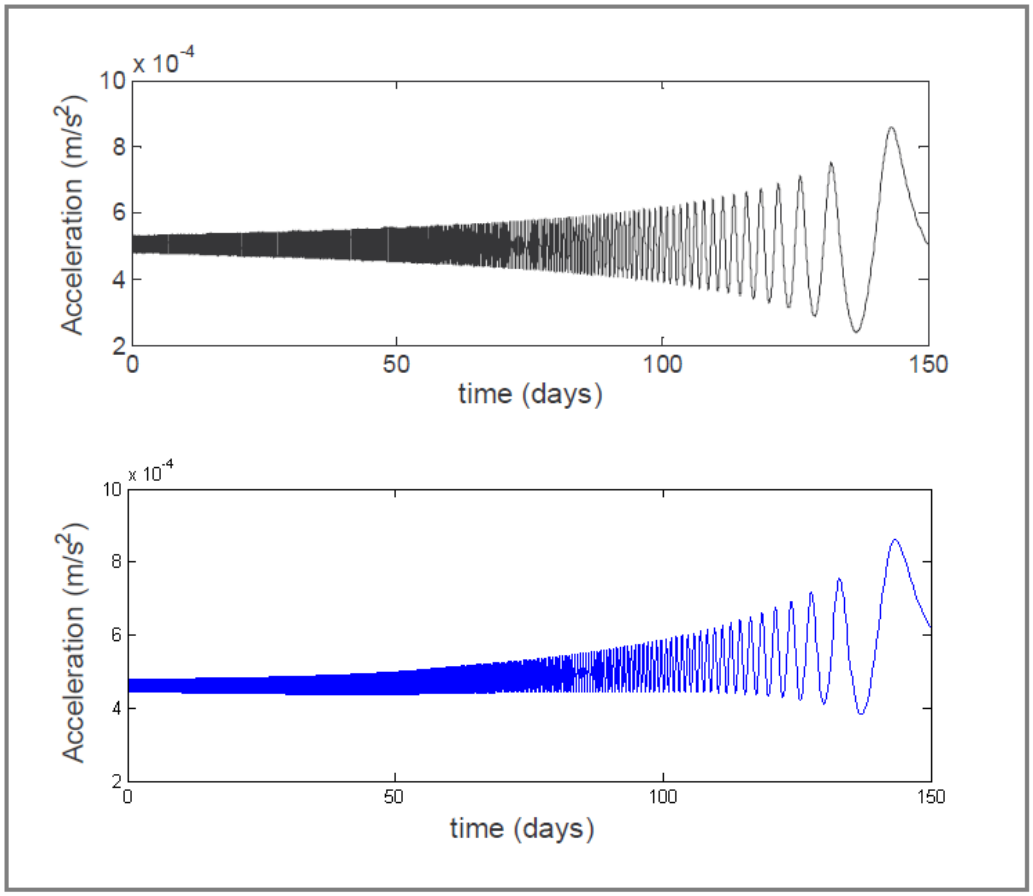

Figure 4.2: Earth escape: acceleration comparison between Ranieri's result *(top)* and Catucci's one *(bottom)*

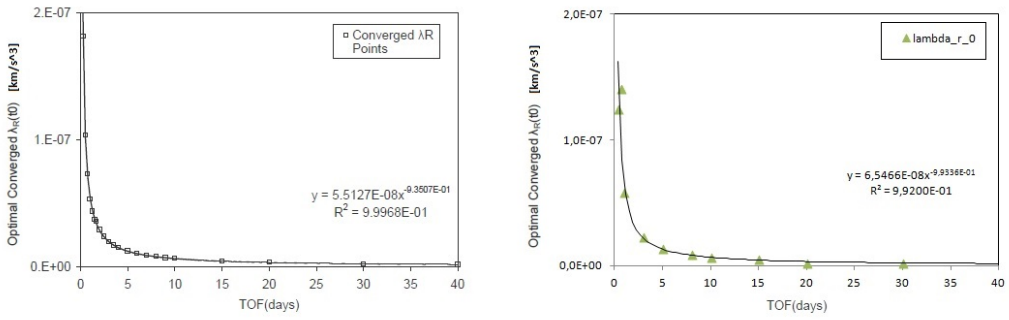

Figure 4.3: Polar Curve Fit for the Earth escape: λ_{r_0} comparison between Ranieri's result *(left)* and Catucci's one *(right)*

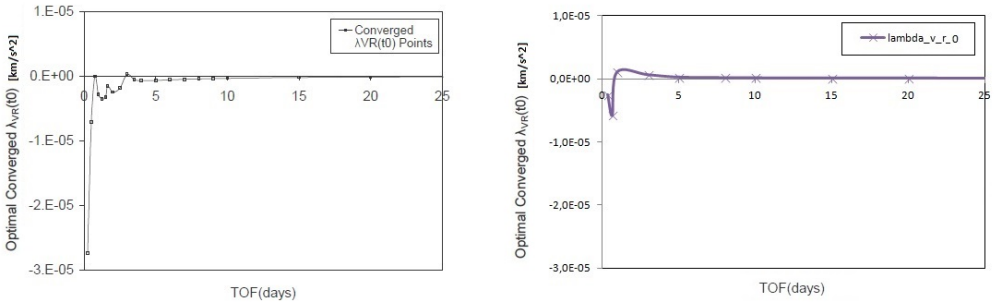

Figure 4.4: Polar Curve Fit for the Earth escape: $\lambda_{v_{r_0}}$ comparison between Ranieri's result *(left)* and Catucci's one *(right)*

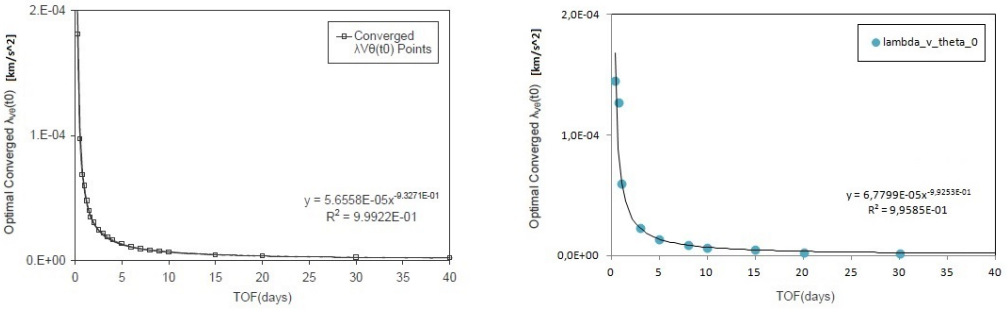

Figure 4.5: Polar Curve Fit for the Earth escape: $\lambda_{v_{\theta_0}}$ comparison between Ranieri's result *(left)* and Catucci's one *(right)*

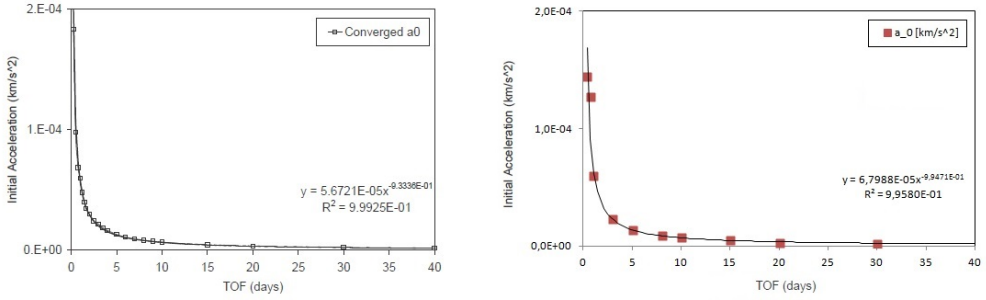

Figure 4.6: Polar Curve Fit for the Earth escape: a_0 comparison between Ranieri's result *(left)* and Catucci's one *(right)*

plane position and velocity variables are always zero, as well as the related co-states. λ_θ, instead, does not appear because it is always equal to zero, as demonstrated in Section 2.1.1.

4.4 LEO-to-LEO transfer

This Section deals with a fuel-optimal transfer (Case B) where a LEO with an altitude h of 2122 km is targeted, starting from a LEO with $h = 500$ km. The spacecraft has an initial mass m_0 of 1000 kg and is supported by five resistojet engines, whose maximum power is $P_{max} = 0.9$ kW and which are not able overall to overcome 0.5 N of thrust.

A *constrained* solution of Case B is so requested and in order to obtain it, the minimum-thrust-acceleration problem (Case A) must be solved before. In the followings, the complete procedure is shown step by step according to the algorithms presented in Sections 3.2 and 3.5.

4.4.1 Solution of Case A

1. Paremeters definition:

$$TOF = 3\,day \tag{4.1}$$

$$\begin{bmatrix} r_0 \\ \theta_0 \\ v_{r_0} \\ v_{\theta_0} \end{bmatrix} = \begin{bmatrix} 6878\,km \\ 0 \\ 0 \\ 7.613\,km/s \end{bmatrix} \tag{4.2}$$

$$toll = 10^{-3} \tag{4.3}$$

$$\begin{bmatrix} r_{tar} \\ v_{r_{tar}} \\ v_{\theta_{tar}} \end{bmatrix} = \begin{bmatrix} 8500\,km \\ 0 \\ 6.848\,km/s \end{bmatrix} \tag{4.4}$$

Observe that as the transfer takes place in the equatorial plane, the variables ϕ and v_ϕ are always null, as well as their co-states. Vectors $\mathbf{x}$ and λ reduce so to:

$$\mathbf{x} = \begin{bmatrix} r \\ \theta \\ v_r \\ v_\theta \end{bmatrix}; \qquad \lambda = \begin{bmatrix} \lambda_r \\ \lambda_\theta \\ \lambda_{v_r} \\ \lambda_{v_\theta} \end{bmatrix} \tag{4.5}$$

2. as there is no targeted theta position θ_{tar}, λ_θ will be always equal to zero. Thus, the resulting unknowns $\mathbf{z}$ and constraints $\mathbf{c}$ are:

$$\mathbf{z} = \begin{bmatrix} \lambda_{r_0} \\ \lambda_{v_{r_0}} \\ \lambda_{v_{\theta_0}} \end{bmatrix}; \qquad \mathbf{c} = \begin{bmatrix} r_f - r_{tar} \\ v_{r_f} - v_{r_{tar}} \\ v_{\theta_f} - v_{\theta_{tar}} \end{bmatrix} = \mathbf{0} \tag{4.6}$$

3. ACT parameters estimation:

   (a) again, as the transfer is planar, the out-of-plane angle γ and its time derivative $\dot{\gamma}$ are always zero; on the other hand, α_0 can be set to $\pi/2$ and $\dot{\alpha}_0$ to zero, for the reasons explained in Section 4.2;

   (b) after few attempts, a good first guess for the initial acceleration a_0 has been found without resorting to the PCF technique. The selected time of flight, indeed, is relatively low and simple shooting converges quite easily to the optimal solution. As a result, a_0 has been set to $3 \cdot 10^{-6}\ km/s^2$;

4. *simple shooting* technique:

   (a) as the matter of facts, the initial thrust angles and acceleration take the place of the initial co-states in the $\mathbf{z}$ vector:

$$\mathbf{z} = \begin{bmatrix} \alpha_0 \\ \dot{\alpha}_0 \\ a_0 \end{bmatrix} \tag{4.7}$$

   The ACT is so performed at each step inside simple shooting in order to compute the co-state vector. For the sake of completeness, the initial co-states resulting by inputing the selected thrust angles and acceleration to the ACT have been evaluated:

$$\begin{bmatrix} \lambda_{r_0} \\ \lambda_{v_{r_0}} \\ \lambda_{v_{\theta_0}} \end{bmatrix} = ACT(\alpha_0, \dot{\alpha}_0, a_0) = \begin{bmatrix} 3.322 \cdot 10^{-9}\ km/s^3 \\ 5.236 \cdot 10^{-8}\ km/s^2 \\ 3.000 \cdot 10^{-6}\ km/s^2 \end{bmatrix} \tag{4.8}$$

   (b) now that all the unknowns have been initialized, *simple shooting* can be run. The ODEs (2.10) and (2.8) are integrated;

   (c) simple shooting tries to optimize the inputed $\mathbf{z}$ in order to get the optimal $\mathbf{z}_{opt}$ that fulfills the constraints $\mathbf{c}$;

5. once simple shooting finishes to work, the optimized unkwnowns $\mathbf{z}_{opt}$ are obtained and the constraints $\mathbf{c}$ are evaluated:

$$\mathbf{z}_{opt} = \begin{bmatrix} \alpha_{0_{opt}} \\ \dot{\alpha}_{0_{opt}} \\ a_{0_{opt}} \end{bmatrix} = \begin{bmatrix} 1.569\, rad \\ 4.220 \cdot 10^{-6}\, rad/s \\ 2.932 \cdot 10^{-6}\, km/s^2 \end{bmatrix} \tag{4.9}$$

$$\mathbf{c} = \begin{bmatrix} r_f - r_{tar} \\ v_{r_f} - v_{r_{tar}} \\ v_{\theta_f} - v_{\theta_{tar}} \end{bmatrix} = 10^{-3} \cdot \begin{bmatrix} 0.389\, km \\ -0.047\, km/s \\ 0.045\, km/s \end{bmatrix} \tag{4.10}$$

The maximum constraint violation is so equal to $0.389 \cdot 10^{-3}\, km$ and is lower than the fixed tollerance *toll*. Consequently, the algorithm jumps to Step 6;

6. optimized initial co-states:

$$\lambda_{\mathbf{0_{opt}}} = \begin{bmatrix} \lambda_{r_{0_{opt}}} \\ \lambda_{v_{r_{0_{opt}}}} \\ \lambda_{v_{\theta_{0_{opt}}}} \end{bmatrix} = ACT(\alpha_{0_{opt}}, \dot{\alpha}_{0_{opt}}, a_{0_{opt}}) = \begin{bmatrix} 3.257 \cdot 10^{-9}\, km/s^3 \\ 5.491 \cdot 10^{-9}\, km/s^2 \\ 3.000 \cdot 10^{-6}\, km/s^2 \end{bmatrix} \tag{4.11}$$

Note that these values are not so far from those estimated with the ACT (Equation (4.8));

7. ODEs (2.10) and (2.8) are integrated starting from $[\mathbf{x}_0, \lambda_{0_{opt}}]$ and $\mathbf{x}(t)$, $\lambda(t)$ are obtained;

8. *multiple shooting* technique:

   (a) the expressions of $\mathbf{x}(t)$, $\lambda(t)$ found with simple shooting are used as first guess for multiple shooting;

   (b) the time span is divided into two intervals, so $N_{int} = 2$. Remind that in the considered transfer only 8 variables are involved (4 states and 4 co-states), so $N_{var} = 8$. Multiple shooting needs a number of boundary conditions **b.c.** equal to $N_{int} \cdot N_{var} = 16$. They are:

$$\mathbf{b.c.} = \begin{bmatrix} r(t_0) - r_0 \\ \theta(t_0) - \theta_0 \\ v_r(t_0) - v_{r_0} \\ v_\theta(t_0) - v_{\theta_0} \\ r(t_f) - r_{tar} \\ v_r(t_f) - v_{r_{tar}} \\ v_\theta(t_f) - v_{\theta_{tar}} \\ r(t/2^-) - r(t/2^+) \\ \theta(t/2^-) - \theta(t/2^+) \\ v_r(t/2^-) - v_r(t/2^+) \\ v_\theta(t/2^-) - v_\theta(t/2^+) \\ \lambda_r(t/2^-) - \lambda_r(t/2^+) \\ \lambda_\theta(t/2^-) - \lambda_\theta(t/2^+) \\ \lambda_{v_r}(t/2^-) - \lambda_{v_r}(t/2^+) \\ \lambda_{v_\theta}(t/2^-) - \lambda_{v_\theta}(t/2^+) \\ a(t/2^-) - a(t/2^+) \end{bmatrix} = \mathbf{0} \tag{4.12}$$

It is worth observing that the original constraints **c** expressed in Equation (4.6) are included in the **b.c.**;

(c) multiple shooting tries to refine the initial guess solution in order to perfectly fit the imposed boundary conditions **b.c.** (and consequently the constraints **c**);

9. once multiple shooting finishes the optimization process, the constraints **c** are evaluated and in this case are all fulfilled according to the multiple-shooting default tollerance, which is equal to 10^{-6}. The solution obtained with multiple shooting represents so the optimal solution of Case A and the algorithm for Case B (Section 3.5) can now be implemented.

4.4.2 Solution of Case B

1. parameters settings:

$$\mathrm{m}_0 = 1000\ kg \tag{4.13}$$

$$\mathrm{P}_{max} = 5\ engine\ \cdot 0.9\ kW/engine = 4.5\ kW \tag{4.14}$$

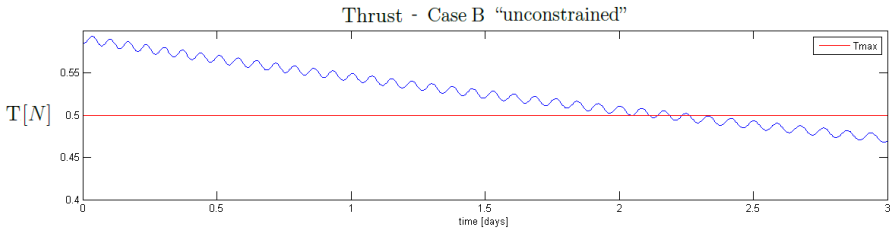

Figure 4.7: Control profile of one resistojet engine for a thrust-unconstrained LEO-to-LEO transfer

2. the control laws for Case A and B are matched (Equation (3.15));

3. thanks to this assumption:

   (a) λ_{m_0} can be set to any positive value, for example one;

   (b) the initial position and velocity co-states are recovered:

$$\lambda_{\mathbf{B_{v,r_0}}} = \begin{bmatrix} \lambda_{B_{r_0}} \\ \lambda_{B_{\theta_0}} \\ \lambda_{B_{v_{r_0}}} \\ \lambda_{B_{v_{\theta_0}}} \end{bmatrix} = \frac{{m_0}^2 \lambda_{m_0}}{P_{max}} \begin{bmatrix} \lambda_{A_{r_0}} \\ \lambda_{A_{\theta_0}} \\ \lambda_{A_{v_{r_0}}} \\ \lambda_{A_{v_{\theta_0}}} \end{bmatrix} = \begin{bmatrix} 7.238 \cdot 10^{-4}\ kg/m \\ 0 \\ 1.220 \cdot 10^{-3}\ kg\ s/m \\ 6.667 \cdot 10^{-1}\ kg\ s/m \end{bmatrix} \tag{4.15}$$

4. ODEs (3.31) and (3.32) are integrated starting from $\mathbf{x}_0$ and $\lambda_{\mathbf{B_0}}$, with $\lambda_{\mathbf{B}0} = [\lambda_{\mathbf{B_{v,r_0}}}; \lambda_{m_0}]$. As a result, the "*unconstrained*" solution is obtained, that is the solution of Case B without control saturation.

   Just looking at the thrust profile of one engine, it is evident that the fixed T_{max} has been overcome (Figure 4.7);

5. let us try to find a "*constrained*" solution, where the maximum achievable thrust for each engine is $T_{max} = 0.5\ N$;

6. multiple shooting techinique is adopted with two time intervals; now $N_{int} = 2$, but $N_{var} = 10$ (five states and five co-states) so 20 boundary conditions are needed:

$$\mathbf{b.c.} = \begin{bmatrix} r(t_0) - r_0 \\ \theta(t_0) - \theta_0 \\ v_r(t_0) - v_{r_0} \\ v_\theta(t_0) - v_{\theta_0} \\ m(t_0) - m_0 \\ \lambda_m(t_0) - \lambda_{m_0} \\ r(t_f) - r_{tar} \\ v_r(t_f) - v_{r_{tar}} \\ v_\theta(t_f) - v_{\theta_{tar}} \\ r(t/2^-) - r(t/2^+) \\ \theta(t/2^-) - \theta(t/2^+) \\ v_r(t/2^-) - v_r(t/2^+) \\ v_\theta(t/2^-) - v_\theta(t/2^+) \\ m(t/2^-) - m(t/2^+) \\ \lambda_r(t/2^-) - \lambda_r(t/2^+) \\ \lambda_\theta(t/2^-) - \lambda_\theta(t/2^+) \\ \lambda_{v_r}(t/2^-) - \lambda_{v_r}(t/2^+) \\ \lambda_{v_\theta}(t/2^-) - \lambda_{v_\theta}(t/2^+) \\ \lambda_m(t/2^-) - \lambda_m(t/2^+) \\ a(t/2^-) - a(t/2^+) \end{bmatrix} = \mathbf{0} \tag{4.16}$$

   (a) the state ODEs are now decoupled from the co-states, expressing them as function of the control variables (Equations (3.34));

   (b) the transformations described in Equations (3.35), (3.36) and (3.37) are performed at each time step, computing so the current value of the thrust (Equation (3.38));

7. if the current thrust is greater than the fixed T_{max}, then:

   (a) the thrust components are re-scaled according to Equations (3.39), (3.40) and (3.41);

   otherwise the procedure skips Step 7.a and goes directly to Step 8:

8. the full set of ODEs (3.31) and (3.32) is integrated till the subsequent time step.

   Passages from Step 6.b are repeated till the final time is reached;

9. multiple shooting succeeds to find the optimal solution as all the **b.c.** (and consequently all the constraints **c**) have been conducted to zero and the control profile of each engine does not overcome T_{max} (Figure 4.8).

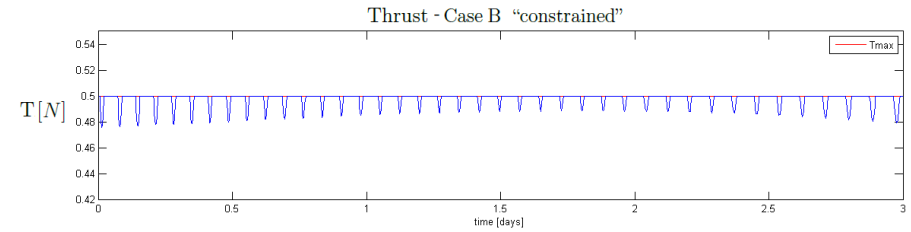

Figure 4.8: Control profile of one resistojet engine for a thrust-constrained LEO-to-LEO transfer

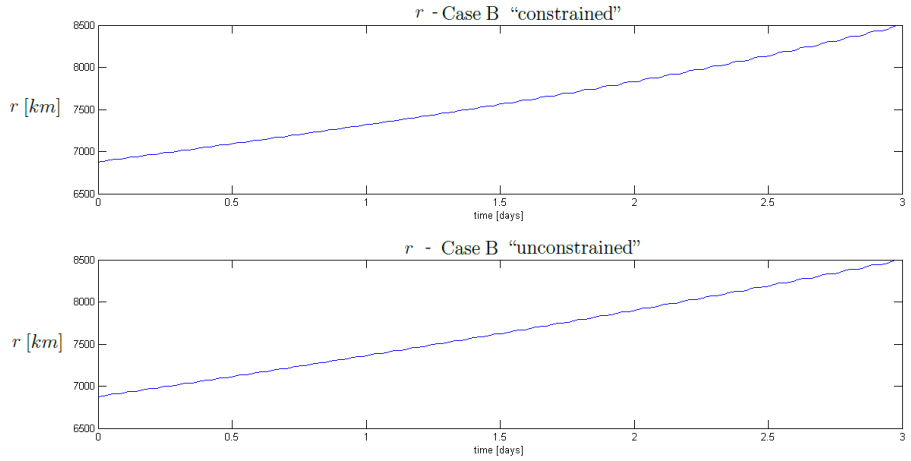

Figure 4.9: r-profile in a LEO-to-LEO transfer in Case B: on the top the constrained solution and on the bottom the unconstrained one. In both the cases, the final value of r matches the target one: 8500 km.

In the followings, all the optimal states and co-states variables are shown for the "unconstrained" and the "constrained" solution of Case B (from Figure 4.9 to 4.14).

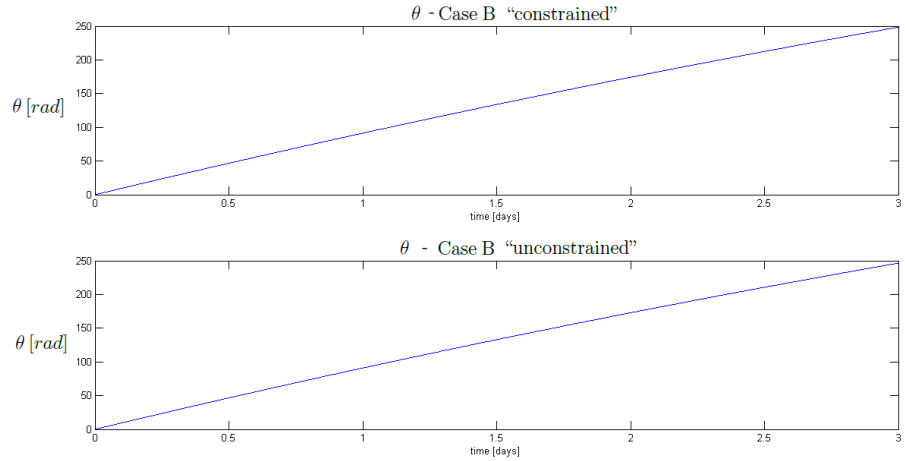

Figure 4.10: θ-profile in a LEO-to-LEO transfer in Case B: on the top the constrained solution and on the bottom the unconstrained one. By dividing the final value of θ by 2π, the number of revolutions can be recovered: 78.9 in the constrained case and 78.5 and in the unconstrained case.

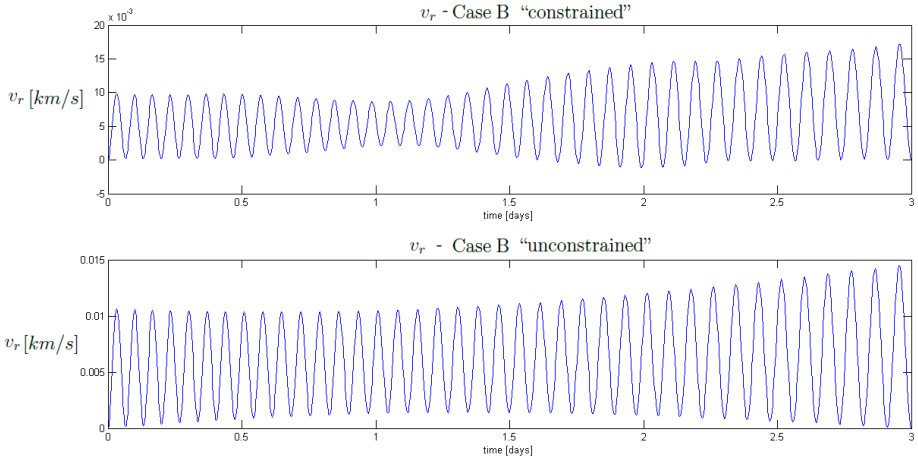

Figure 4.11: v_r-profile in a LEO-to-LEO transfer in Case B: on the top the constrained solution and on the bottom the unconstrained one. In both the cases, the initial and the final values of v_r are equal to zero, as the starting and the target orbits are circular.

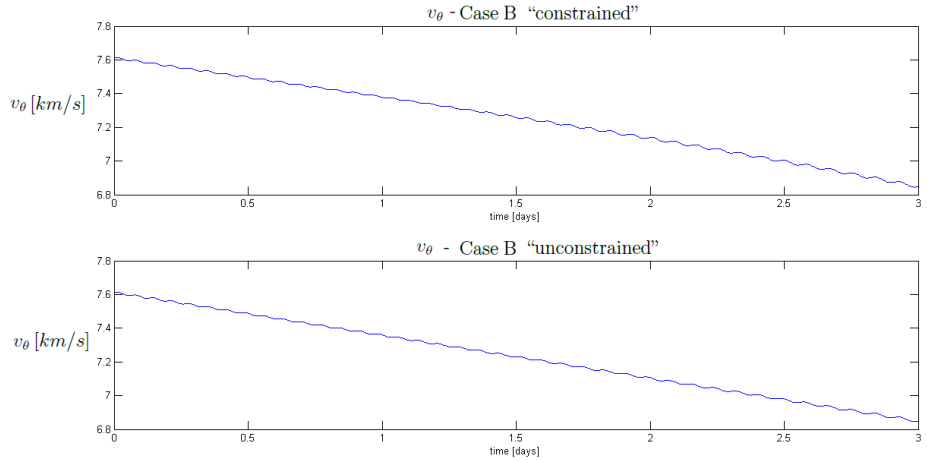

Figure 4.12: v_θ-profile in a LEO-to-LEO transfer in Case B: on the top the constrained solution and on the bottom the unconstrained one. In both the cases, the final value of v_θ matches the target one: 6.848 km/s.

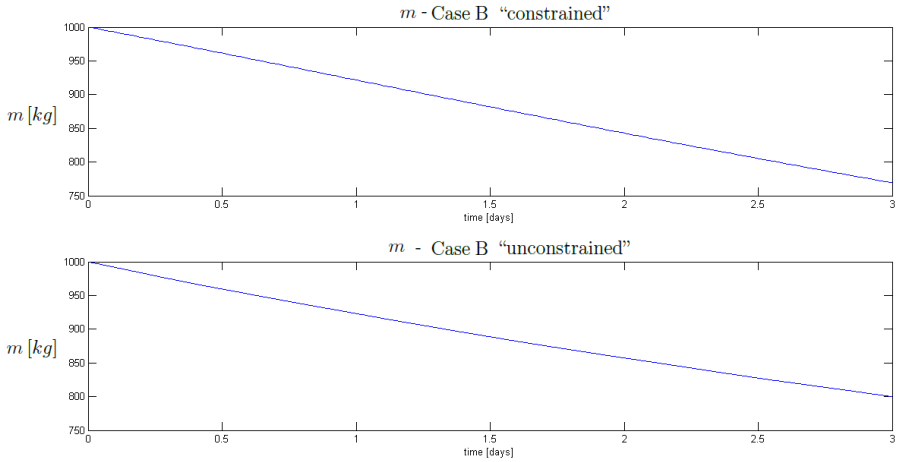

Figure 4.13: m-profile in a LEO-to-LEO transfer in Case B: on the top the constrained solution and on the bottom the unconstrained one. It is worth observing that the imposition of the control saturation allows a greater propellant saving.

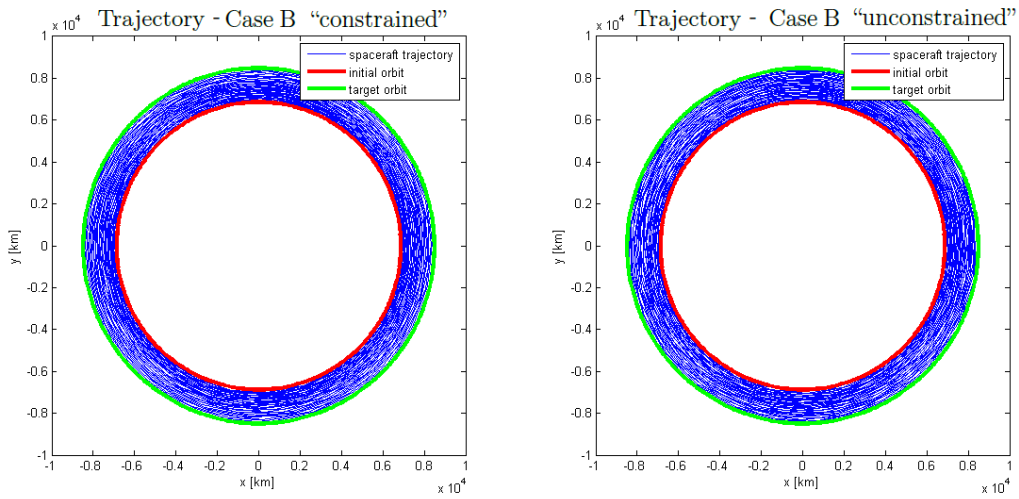

Figure 4.14: Trajectory performed in a LEO-to-LEO transfer in Case B: on the left the constrained solution and on the right the unconstrained one

4.4.3 Sensitivity to the maximum thrust

The sensitivity to the maximum thrust is investigated in this section. Particularly, the LEO-to-LEO transfer has been performed with four different values of maximum thrust. In Figure 4.15, from top to bottom, T_{max} has been fixed to: 0.50 N, 0.52 N, 0.53 N and 0.55 N.

It is particularly interesting to compare the two cases on the top, where an increase of T_{max} from 0.50 N to 0.52 N involves a reduction of the oscillatory behaviour of the thrust: as the matter of facts, the transfer with $T_{max} = 0.52$ N is performed with a thrust profile almost constant in time.

On the other hand, comparing the two cases on the bottom shows that the lower the maximum achievable thrust is, the more the "plateau" region delates, as a greater control effort is needed to perform the transfer.

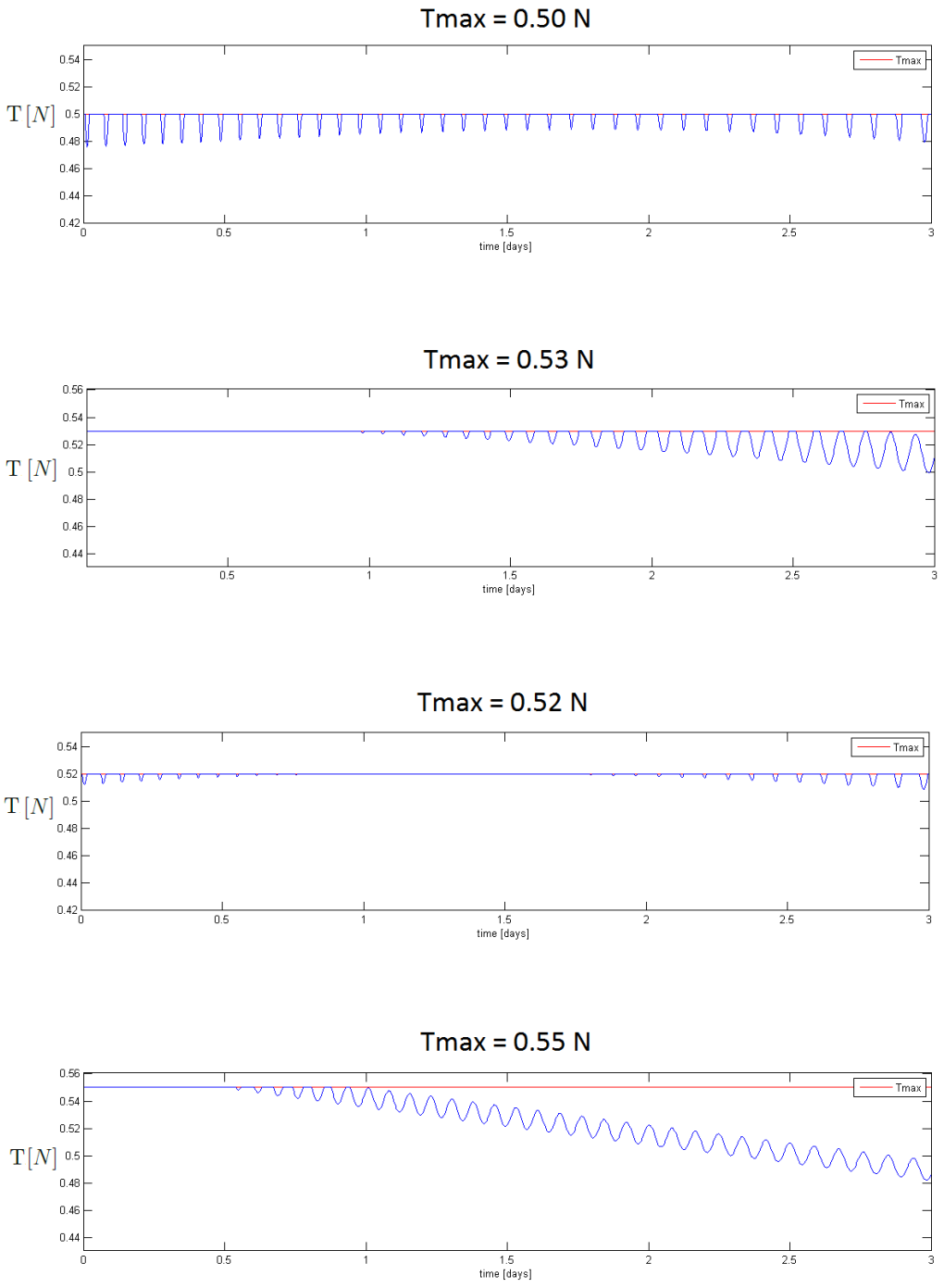

Figure 4.15: Constrained solution of Case B for a LEO-to-LEO transfer with different T_{max}. From top to bottom the thrust profiles with: $T_{max} = 0.50\ N$, $T_{max} = 0.52\ N$, $T_{max} = 0.53\ N$ and $T_{max} = 0.55\ N$

4.5 LEO-to-GEO transfer

This section deals with a fuel-optimal transfer (Case B) where a GEO is targeted, starting from a LEO with $h = 500\ km$. The spacecraft has an initial mass m_0 of 1000 kg and is supported by three resistojet engines, whose maximum power is $P_{max} = 1.2\ kW$ and which are not able to overcome 0.5 N of thrust.

A *constrained* solution of Case B is so requested and in order to obtain it, the minimum-thrust-acceleration problem (Case A) must be solved first. In the followings, the complete procedure shown step by step according to the algorithms presented in Sections 3.2 and 3.5.

4.5.1 Solution of Case A

1. Paremeters definition:

$$TOF = 30\ day \tag{4.17}$$

$$\begin{bmatrix} r_0 \\ \theta_0 \\ v_{r_0} \\ v_{\theta_0} \end{bmatrix} = \begin{bmatrix} 6878\ km \\ 0 \\ 0 \\ 7.613\ km/s \end{bmatrix} \tag{4.18}$$

$$toll = 10^{-1} \tag{4.19}$$

$$\begin{bmatrix} r_{tar} \\ v_{r_{tar}} \\ v_{\theta_{tar}} \end{bmatrix} = \begin{bmatrix} 42168\ km \\ 0 \\ 3.075\ km/s \end{bmatrix} \tag{4.20}$$

Furthermore the transfer takes place in the equatorial plane, so the variables ϕ and v_ϕ are always zero, as well as their co-states. Vectors $\mathbf{x}$ and λ reduce consequently to:

$$\mathbf{x} = \begin{bmatrix} r \\ \theta \\ v_r \\ v_\theta \end{bmatrix}; \qquad \lambda = \begin{bmatrix} \lambda_r \\ \lambda_\theta \\ \lambda_{v_r} \\ \lambda_{v_\theta} \end{bmatrix} \tag{4.21}$$

2. as there is no targeted theta position θ_{tar}, λ_θ will be always equal to zero. The resulting unknowns $\mathbf{z}$ and constraints $\mathbf{c}$ are so:

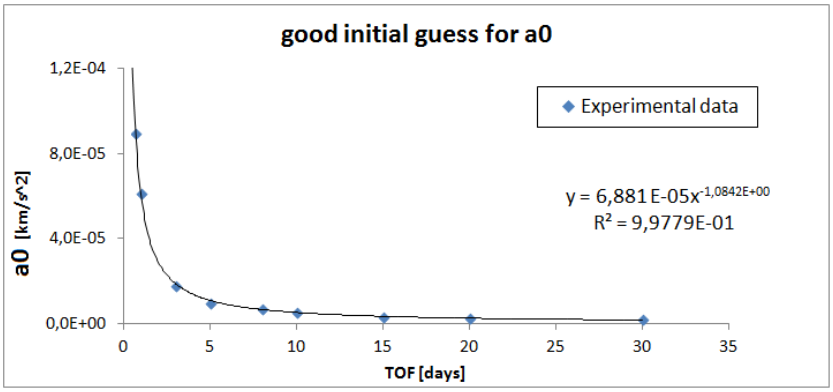

Figure 4.16: Polar Curve Fit for the initial acceleration a_0 of a LEO-to-GEO transfer in Case A

$$\mathbf{z} = \begin{bmatrix} \lambda_{r_0} \\ \lambda_{v_{r_0}} \\ \lambda_{v_{\theta_0}} \end{bmatrix}; \qquad \mathbf{c} = \begin{bmatrix} r_f - r_{tar} \\ v_{r_f} - v_{r_{tar}} \\ v_{\theta_f} - v_{\theta_{tar}} \end{bmatrix} = \mathbf{0} \tag{4.22}$$

3. ACT parameters estimation:

   (a) again, as the transfer is planar, the out-of-plane angle γ and its time derivative $\dot{\gamma}$ are always zero; on the other hand, α_0 can be set to $\pi/2$ and $\dot{\alpha}_0$ to zero, for the reasons explained in Section 4.2;

   (b) after few attempts, it was clear that finding a good first guess for the initial acceleration a_0 was not easy. The selected time of flight, indeed, is relatively high and simple shooting can converge only with a very accurate first guess. For this reason, steps from 5.a to 5.c have been performed resorting to the PCF technique. The produced curve, shown in Figure 4.16, takes the following form: $y = 6.811 \cdot 10^{-5} \cdot x^{-1.0842}$, where x represents the time of flight, expressed in *day*, and y the accurate first guess of the initial acceleration, expressed in km/s^2. As a result, a_0 has been set to $1.705 \cdot 10^{-6}\ km/s^2$ for the considered transfer ($x = 30\ day$);

4. *simple shooting* technique:

   (a) as the matter of facts, the initial thrust angles and acceleration take the place of the initial co-states in the $\mathbf{z}$ vector:

$$\mathbf{z} = \begin{bmatrix} \alpha_0 \\ \dot{\alpha}_0 \\ a_0 \end{bmatrix} \tag{4.23}$$

The ACT is so performed at every time step inside simple shooting in order to compute the co-state vector. For the sake of completeness, the initial co-states resulting by inputing the selected thrust angles and acceleration to the ACT have been evaluated:

$$\begin{bmatrix} \lambda_{r_0} \\ \lambda_{v_{r_0}} \\ \lambda_{v_{\theta_0}} \end{bmatrix} = ACT(\alpha_0, \dot{\alpha}_0, a_0) = \begin{bmatrix} 1.888 \cdot 10^{-9}\ km/s^3 \\ 2.976 \cdot 10^{-8}\ km/s^2 \\ 1.705 \cdot 10^{-6}\ km/s^2 \end{bmatrix} \tag{4.24}$$

(b) now that all the unknowns have been initialized, *simple shooting* can be run. The ODEs (2.10) and (2.8) are integrated;

(c) simple shooting tries to optimize $\mathbf{z}$ in order to get the optimal $\mathbf{z}_{opt}$ that fulfills the constraints $\mathbf{c}$;

5. once simple shooting finishes, the optimized unkwnowns $\mathbf{z}_{opt}$ are obtained and the constraints $\mathbf{c}$ are evaluated:

$$\mathbf{z}_{opt} = \begin{bmatrix} \alpha_{0_{opt}} \\ \dot{\alpha}_{0_{opt}} \\ a_{0_{opt}} \end{bmatrix} = \begin{bmatrix} 1.553\ rad \\ -3.661 \cdot 10^{-6}\ rad/s \\ 1.706 \cdot 10^{-6}\ km/s^2 \end{bmatrix} \tag{4.25}$$

$$\mathbf{c} = \begin{bmatrix} r_f - r_{tar} \\ v_{r_f} - v_{r_{tar}} \\ v_{\theta_f} - v_{\theta_{tar}} \end{bmatrix} = 10^{-1} \cdot \begin{bmatrix} 0.0001\ km \\ 0.844\ km/s \\ -0.946\ km/s \end{bmatrix} \tag{4.26}$$

The maximum constraint violation is so equal to $0.946 \cdot 10^{-1}\ km/s$ and is lower than the fixed tollerance *toll*. Consequently, the algorithm jumps to Step 6. As shown in the next step, multiple shooting will be able to lead to zero all the constraints;

6. optimized initial co-states:

$$\lambda_{\mathbf{0_{opt}}} = \begin{bmatrix} \lambda_{r_{0_{opt}}} \\ \lambda_{v_{r_{0_{opt}}}} \\ \lambda_{v_{\theta_{0_{opt}}}} \end{bmatrix} = ACT(\alpha_{0_{opt}}, \dot{\alpha}_{0_{opt}}, a_{0_{opt}}) = \begin{bmatrix} 1.889 \cdot 10^{-9}\ km/s^3 \\ 2.977 \cdot 10^{-8}\ km/s^2 \\ 1.706 \cdot 10^{-6}\ km/s^2 \end{bmatrix} \tag{4.27}$$

Note that these values are very close to those estimated with the ACT (Equation (4.24));

7. ODEs (2.10) and (2.8) are integrated starting from $[\mathbf{x}_0,\lambda_{0_{opt}}]$ and $\mathbf{x}(t)$, $\lambda(t)$ are obtained;

8. *multiple shooting* technique:

   (a) the expressions of $\mathbf{x}(t)$, $\lambda(t)$ found with simple shooting are used as first guess for multiple shooting;

   (b) the time span is divided into two intervals, so $N_{int} = 2$. Remind that in the considered transfer only 8 variables are involved (4 states and 4 co-states), so $N_{var} = 8$. Multiple shooting needs a number of boundary conditions **b.c.** equal to $N_{int} \cdot N_{var} = 16$. They are:

$$\mathbf{b.c.} = \begin{bmatrix} r(t_0) - r_0 \\ \theta(t_0) - \theta_0 \\ v_r(t_0) - v_{r_0} \\ v_\theta(t_0) - v_{\theta_0} \\ r(t_f) - r_{tar} \\ v_r(t_f) - v_{r_{tar}} \\ v_\theta(t_f) - v_{\theta_{tar}} \\ r(t/2^-) - r(t/2^+) \\ \theta(t/2^-) - \theta(t/2^+) \\ v_r(t/2^-) - v_r(t/2^+) \\ v_\theta(t/2^-) - v_\theta(t/2^+) \\ \lambda_r(t/2^-) - \lambda_r(t/2^+) \\ \lambda_\theta(t/2^-) - \lambda_\theta(t/2^+) \\ \lambda_{v_r}(t/2^-) - \lambda_{v_r}(t/2^+) \\ \lambda_{v_\theta}(t/2^-) - \lambda_{v_\theta}(t/2^+) \\ a(t/2^-) - a(t/2^+) \end{bmatrix} = \mathbf{0} \tag{4.28}$$

   It is worth observing that the original constraints **c** expressed in Equation (4.22) are included in the **b.c.**;

   (c) multiple shooting tries to refine the initial guess solution in order to perfectly fit the imposed boundary conditions **b.c.** (and consequently the constraints **c**);

9. once multiple shooting finishes the optimization process, the constraints **c** are evaluated and in this case are all fulfilled according to the multiple-shooting default tollerance, which is set to 10^{-6}. The solution obtained with multiple shooting represents so the optimal solution of Case A and the algorithm for Case B (Section 3.5) can now be implemented.

4.5.2 Solution of Case B

1. parameters settings:

   $$\mathrm{m}_0 = 1000\ kg \quad (4.29)$$

   $$\mathrm{P}_{max} = 3\ engine\ \cdot 1.2\ kW/engine = 3.6\ kW \quad (4.30)$$

2. the control laws for Case A and B are matched (Equation (3.15));

3. thanks to this assumption:

   (a) λ_{m_0} can be set to any positive value, for example one;

   (b) the initial position and velocity co-states are recovered:

   $$\lambda_{\mathbf{B_{v,r_0}}} = \begin{bmatrix} \lambda_{B_{r_0}} \\ \lambda_{B_{\theta_0}} \\ \lambda_{B_{v_{r_0}}} \\ \lambda_{B_{v_{\theta_0}}} \end{bmatrix} = \frac{{m_0}^2 \lambda_{m_0}}{P_{max}} \begin{bmatrix} \lambda_{A_{r_0}} \\ \lambda_{A_{\theta_0}} \\ \lambda_{A_{v_{r_0}}} \\ \lambda_{A_{v_{\theta_0}}} \end{bmatrix} = \begin{bmatrix} 9.047 \cdot 10^{-4}\ kg/m \\ 0 \\ 1.525 \cdot 10^{-3}\ kg\ s/m \\ 8.144 \cdot 10^{-1}\ kg\ s/m \end{bmatrix} \quad (4.31)$$

4. ODEs (3.31) and (3.32) are integrated starting from $\mathbf{x}_0$ and $\lambda_{\mathbf{B_0}}$, with $\lambda_{\mathbf{B}0} = [\lambda_{\mathbf{B_{v,r_0}}}; \lambda_{m_0}]$. As a result, the "*unconstrained*" solution is obtained, that is the solution of Case B without control saturation.

   Just looking at the thrust profile of one engine, it is evident that the fixed T_{max} has been overcome (Figure 4.17);

5. let us try to find a "*constrained*" solution, where the maximum achievable thrust for each engine is $T_{max} = 0.5\ N$;

6. multiple shooting techinique is adopted with two time intervals; now $N_{int} = 2$, but $N_{var} = 10$ (five states and five co-states) so 20 boundary conditions are needed:

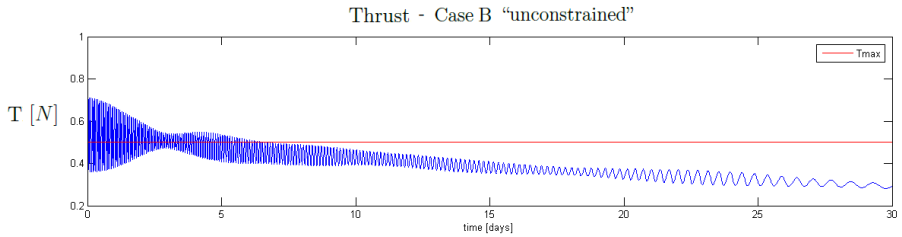

Figure 4.17: Control profile of one resistojet engine for a thrust-unconstrained LEO-to-GEO transfer

$$\mathbf{b.c.} = \begin{bmatrix} r(t_0) - r_0 \\ \theta(t_0) - \theta_0 \\ v_r(t_0) - v_{r_0} \\ v_\theta(t_0) - v_{\theta_0} \\ m(t_0) - m_0 \\ \lambda_m(t_0) - \lambda_{m_0} \\ r(t_f) - r_{tar} \\ v_r(t_f) - v_{r_{tar}} \\ v_\theta(t_f) - v_{\theta_{tar}} \\ r(t/2^-) - r(t/2^+) \\ \theta(t/2^-) - \theta(t/2^+) \\ v_r(t/2^-) - v_r(t/2^+) \\ v_\theta(t/2^-) - v_\theta(t/2^+) \\ m(t/2^-) - m(t/2^+) \\ \lambda_r(t/2^-) - \lambda_r(t/2^+) \\ \lambda_\theta(t/2^-) - \lambda_\theta(t/2^+) \\ \lambda_{v_r}(t/2^-) - \lambda_{v_r}(t/2^+) \\ \lambda_{v_\theta}(t/2^-) - \lambda_{v_\theta}(t/2^+) \\ \lambda_m(t/2^-) - \lambda_m(t/2^+) \\ a(t/2^-) - a(t/2^+) \end{bmatrix} = \mathbf{0} \tag{4.32}$$

(a) the state ODEs are now decoupled from the co-states, expressing them as function of the control variables (Equations (3.34));

(b) the transformations described in Equations (3.35), (3.36) and (3.37) are performed at each time step, computing so the current value of the thrust (Equation (3.38));

7. if the current thrust is greater than the fixed T_{max}, then:

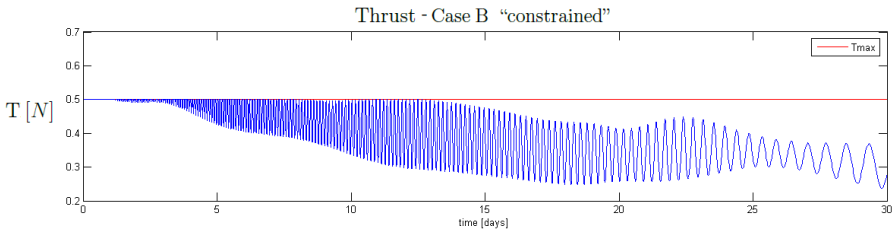

Figure 4.18: Control profile of one resistojet engine for a thrust-constrained LEO-to-GEO transfer

(a) the thrust components are re-scaled according to Equations (3.39), (3.40) and (3.41);

otherwise the procedure skips Step 7.a and goes directly to Step 8:

8. the full set of ODEs (3.31) and (3.32) is integrated till the subsequent time step.

   Passages from Step 6.b are repeated till the final time is reached;

9. multiple shooting has succeeds to find the optimal solution and the **b**.**c**. (and consequently all the constraints **c**) have been conducted to zero and the control profile of each engine does not overcome T_{max} anymore (Figure 4.18).

It is interesting to note that the thrust magnitude is oscillating and that the frequency of the oscillations decreases in time. This seems to suggest the existence of a relation between the thrust frequency and the distance from the main attractor, the Earth. This is confirmed by Figure 4.19, which shows a particular of the constrained thrust profile: the period of the last oscillation is equal to the period of the target orbit, that is one day.

In the followings, all the optimal states and co-states variables are shown for the "unconstrained" and the "constrained" solution of Case B (from Figure 4.20 to 4.25).

4.5.3 Sensitivity to the time of flight

The transfer has been performed with other three different times of flight (TOF) to show the differences in the control law when an upper bound of 0.5 N is imposed to the thrust. Figure 4.26 highlights the sensitivity to the selected time of flight, when it is equal to (from top-left to bottom-right) 28.4 *day*, 30.0 *day*, 32.5 *day* and 34.0 *day*. It is interesting to note that if a

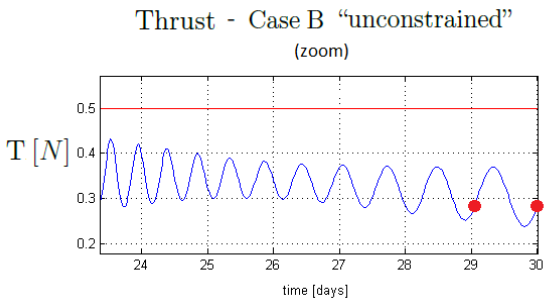

Figure 4.19: Detail of the thrust trend in the LEO-to-GEO transfer. The two red points bound the last oscillation period of the thrust profile, which is very close to 1 *day*

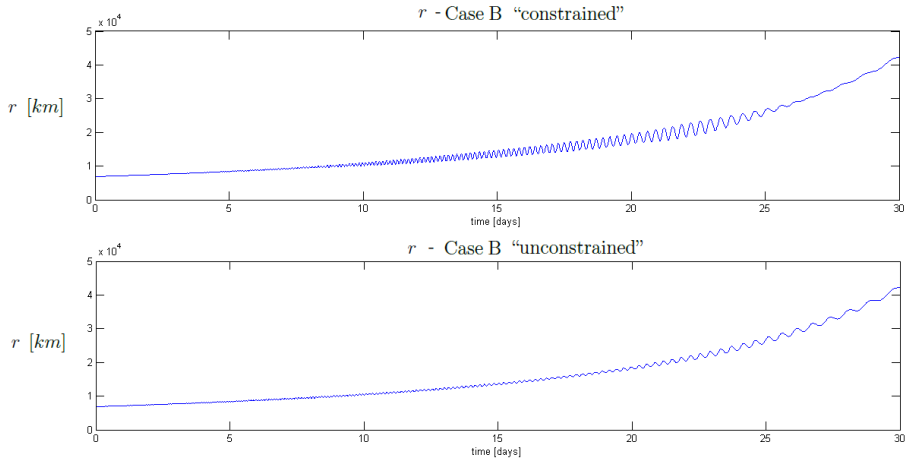

Figure 4.20: r-profile in a LEO-to-GEO transfer in Case B: on the top the constrained solution and on the bottom the unconstrained one. In both the cases, the final value of r matches the target one: 42168 km.

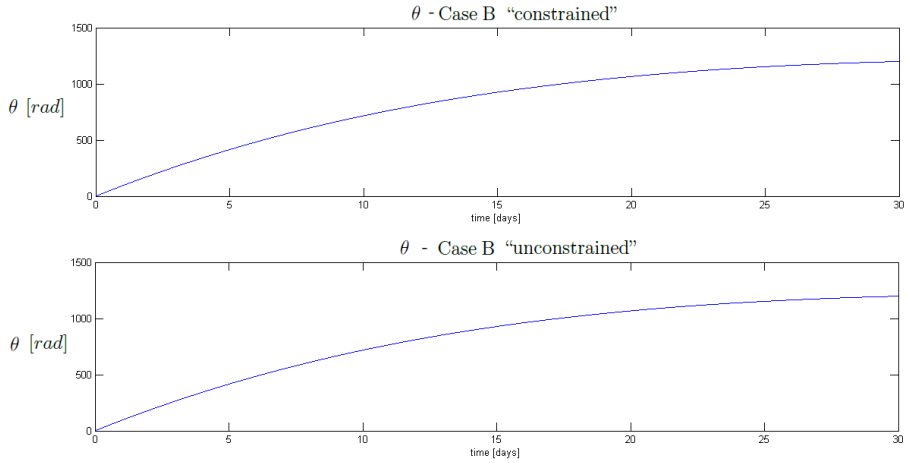

Figure 4.21: θ-profile in a LEO-to-GEO transfer in Case B: on the top the constrained solution and on the bottom the unconstrained one. By dividing the final value of θ by 2π, the number of revolutions can be recovered: 381.8 in the constrained case and 381.5 and in the unconstrained case.

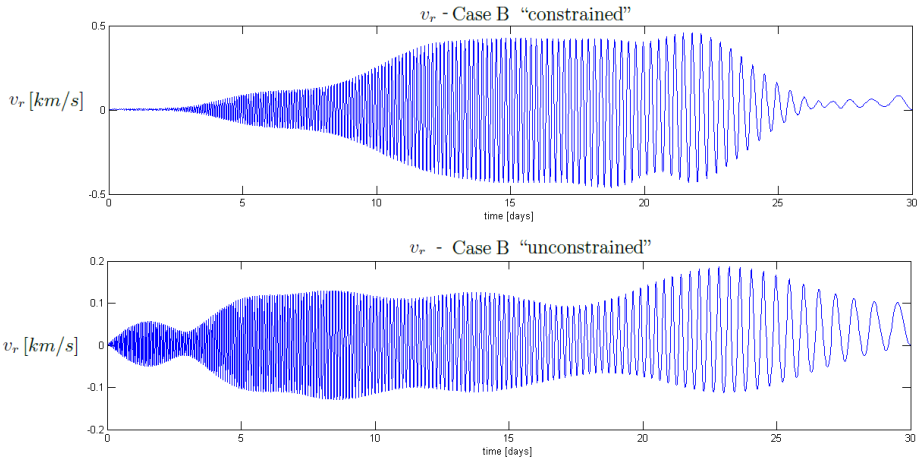

Figure 4.22: v_r-profile in a LEO-to-GEO transfer in Case B: on the top the constrained solution and on the bottom the unconstrained one. In both the cases, the initial and the final values of v_r are equal to zero, as the starting and the target orbits are circular.

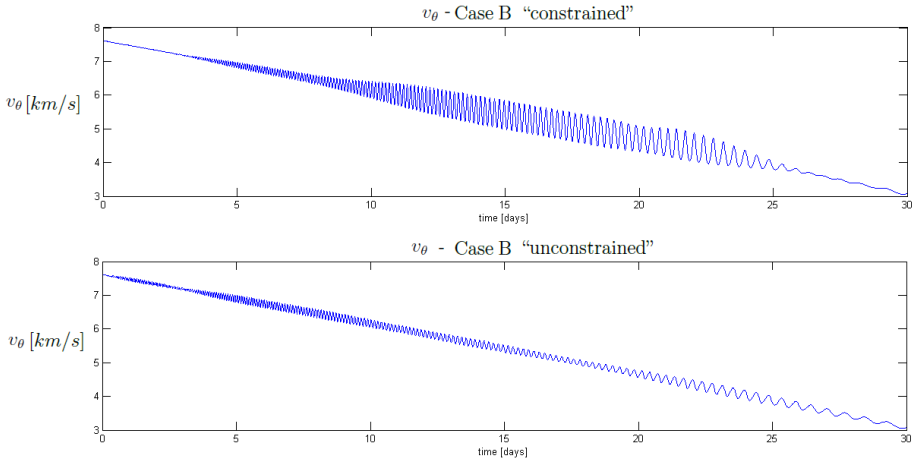

Figure 4.23: v_θ-profile in a LEO-to-GEO transfer in Case B: on the top the constrained solution and on the bottom the unconstrained one. In both the cases, and the final value of v_θ matches the target one: 3.075 km/s.

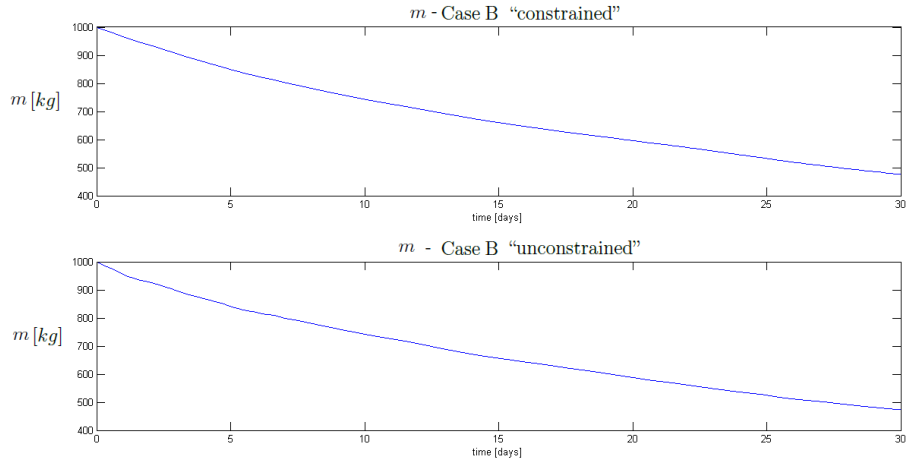

Figure 4.24: m-profile in a LEO-to-GEO transfer in Case B: on the top the constrained solution and on the bottom the unconstrained one. The imposition of the control saturation allows a greater propellant saving as the final mass of the spacecraft is equal to 476.6 kg in the constrained case and 472.9 kg to in the unconstrained one.

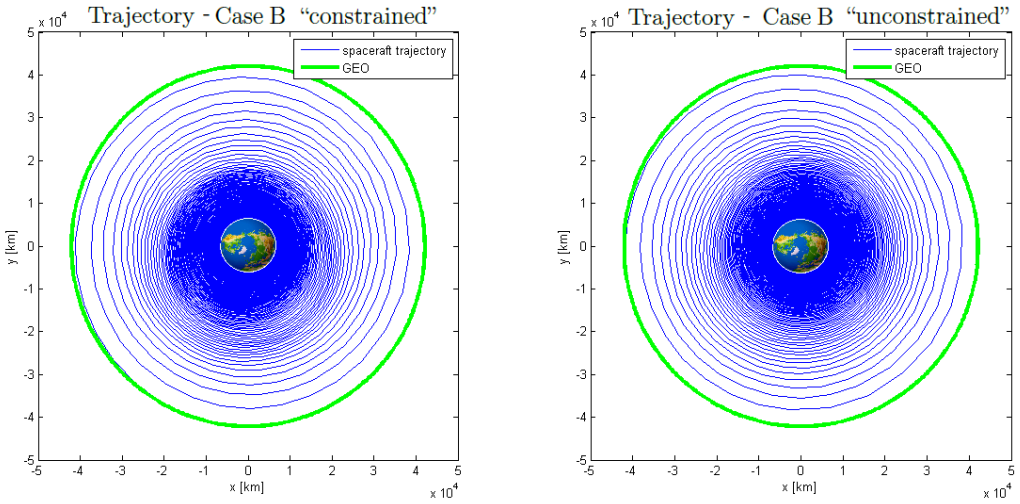

Figure 4.25: Trajectory performed in a LEO-to-GEO transfer in Case B: on the left the constrained solution and on the right the unconstrained one

lower time is available to achieve the target orbit, then the maximum thrust is used for a longer period along the transfer. This can be noted from the figure by looking at the lenght of the "plateau", the region where the thrust equals its maximum level.

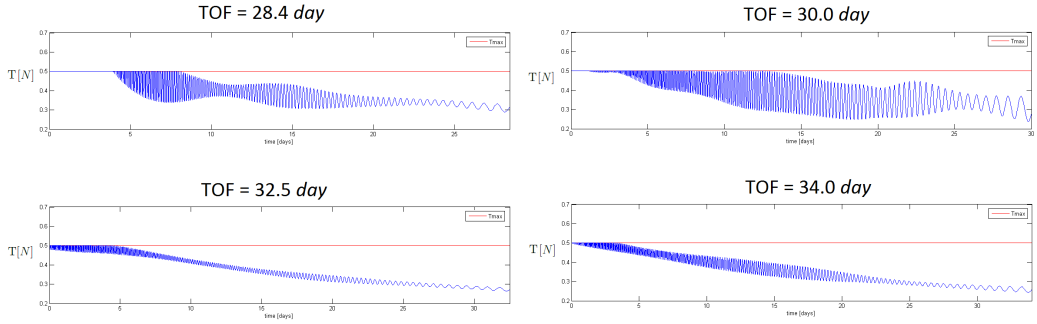

Figure 4.26: Constrained solution of Case B ($T_{max} = 0.5\ N$) for a LEO-to-GEO transfer performed (from top-left to bottom-right) in 28.4 *day*, 30.0 *day*, 32.5 *day* and 34.0 *day* (bottom).

4.6 Earth-to-Mars transfer

A fuel-optimal Earth-to-Mars transfer (Case B) is now investigated with two kinds of thrusters: a typical resistojet and a futuristc nuclear-reactor engine, the "VASIMR" (Variable Specific Impulse Magnetoplasma Rocket). It has been conceived by Chang-Dyaz [21] in the '70s but works are still in progress to make the use of this engine feasible. "Ad Astra", the VASIMR producer, signed an agreement with NASA to arrange the placement and testing of a 200-kW flight version of the VASIMR, the *VF-200*, on the International Space Station (ISS) in 2015. NASA Administrator Charles Bolden said that VASIMR technology could be the breakthrough technology that would reduce travel time on a Mars mission from 2.5 years to 5 months [19]. The VASIMR, indeed, has been conceived with the hope of making feasible manned interplanetary missions. This implies that all the transfers must be performed as fast as possible. As shown in the following, reducing the transfer time to 90 *day* for an Earth-to-Mars mission with a spacecraft capable of hosting humans would require a 10-MW engine (with $m_0 = 10^5\ kg$). There is consequently only one possible source: nuclear. In the past, nuclear electricity has generally been obtained from RTGs, which rely on the heat generated by the natural radioactive decay of plutonium. Such devices have proved crucial to robotic space missions but are too inefficient for human flight. Far better would be a nuclear reactor, which relies on the fission of uranium in a chain reaction. For each kilogram of fuel, a reactor produces up to 10 million times more power than an RTG does [20]. It is clear that the nuclear reactor technology required for such mission is not available today and major advances in reactor design and power conversion are needed. However, a number of serious research studies have been conducted that point to reactor and power

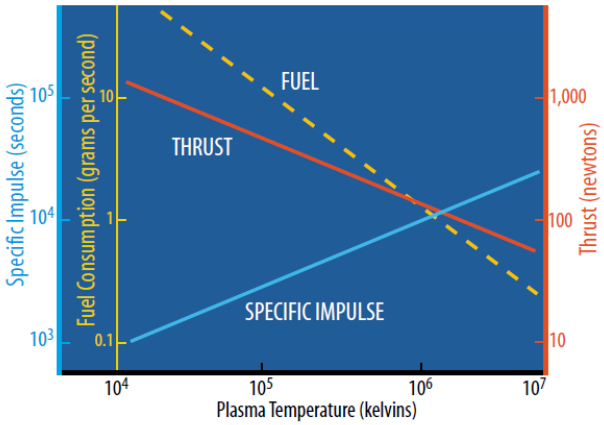

Figure 4.27: Performances expected by a 10-MW VASIMR engine. By increasing its temperature, it boosts its specific impulse (blue) and reduces fuel consumption (yellow) at the price of less thrust (red)

conversion designs that meet the kg/kW required for such a mission [21].

Waiting for this to become real, the Earth-to-Mars test case has been conducted in order to define a mass-power budget.

As a result, the Earth-to-Mars test case has been performed with:

- one VASIMR engine with $P_{max} = 10\ MW$, $m_0 = 10^5\ kg$, $T_{max} = 1000\ N$, TOF=90 day;
- one resistojet thruster with $P_{max} = 1\ kW$, $m_0 = 6 \cdot 10^2\ kg$, $T_{max} = 0.5\ N$, TOF=250 day;
- six resistojet thrusters with $P_{max} = 1\ kW$, $m_0 = 10^4\ kg$, $T_{max} = 0.5\ N$, TOF=350 day;

As for the resistojets, they cannot overcome 0.5 N and so a constrained-Case-B solution was requested to make the transfer possible for the 10^4-kg spacecraft, whereas an unconstrained-Case-B solution resulted sufficient to optimize the transer with the 600-kg spacecraft. An initial mass of 10^5-kg has been instead selected for the VASIMR-engine spacecraft, as it has to host a nuclear reactor, apart from the human crew.

The VASIMR engine can achieve very high levels of thrust and the performances expected by a 10-MW engine are reported in Figure 4.27, taken from [21].

As a consequence, T_{max} has been fixed to $10^3\ N$ but the VASIMR-engine spacecraft never overcame this value, so an unconstrained-Case-B solution was adopted.

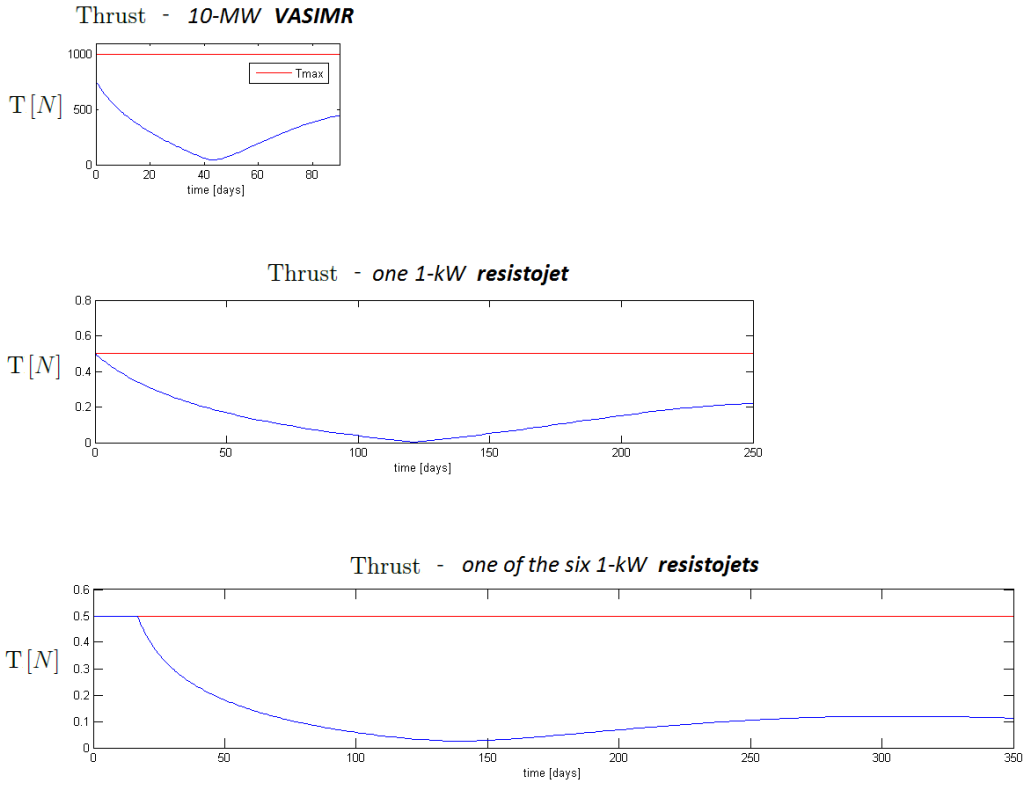

Figure 4.28: Thrust profiles in an Earth-to-Mars transfer obtained with (from top to bottom) the 10-MW VASIMR engine, the 1-kW resistojet used for the 250-*day* transfer, one of the six 1-kW resistojets used for the 350-*day* transfer.

In the test case, only the gravitational field of the Sun is considered, while Earth and Mars are treated as point-masses whose orbits around the Sun are assumed to be circular and co-planar.

As the previous test cases presented in Sections 4.4 and 4.5 have already shown in detail how to follow the Case-A and Case-B algorithms, the dissertation will now focus only on the relevant results, comparing the solutions obtained with the three different engines.

Figure 4.28 shows the thrust profiles, highlighting the completely different orders of magnitude.

Figure 4.29 shows the trajectory performed in the three cases. Observe that with a VASIMR-engine spacecraft, the transfer lasts only 90 *day*. On the other hand, the resistojet-engine spacecrafts are considerably less-power demanding, but they need more time to achieve the Mars orbit. Nevertheless, in all the cases the transfer does not complete even one revolution around

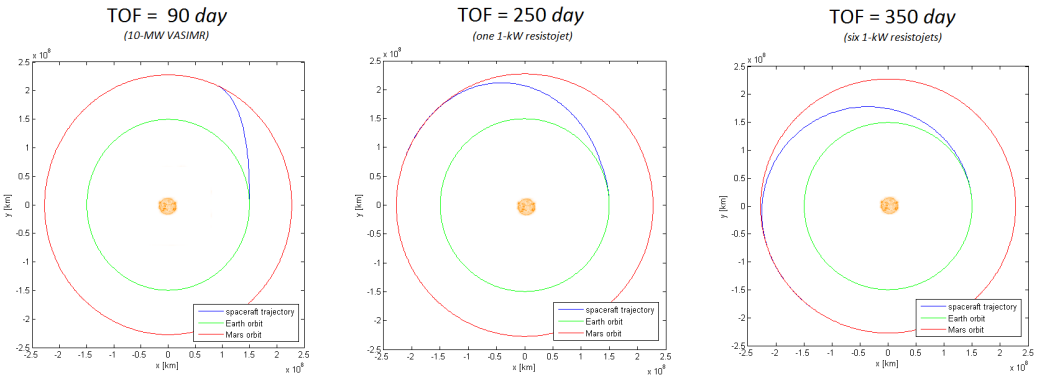

Figure 4.29: Earth-to-Mars transfer obtained (from left to right) with the VASIMR-engine spacecraft (TOF=90 *day*), the one-resistojet-engine spacecraft (TOF=250 *day*), the six-resistojet-engine spacecraft (TOF=350 *day*).

the Sun. As no spiral dynamics is involved, the method presented in Sections 3.2 and 3.5 converged very easily to the optimal solution.

Fiugre 4.30 that shows the mass trends. As for the resistojet-engine spacecrafts, it is worth observing that the tax to be payed for a greater payload mass is a higher transfer time and a greater power source.

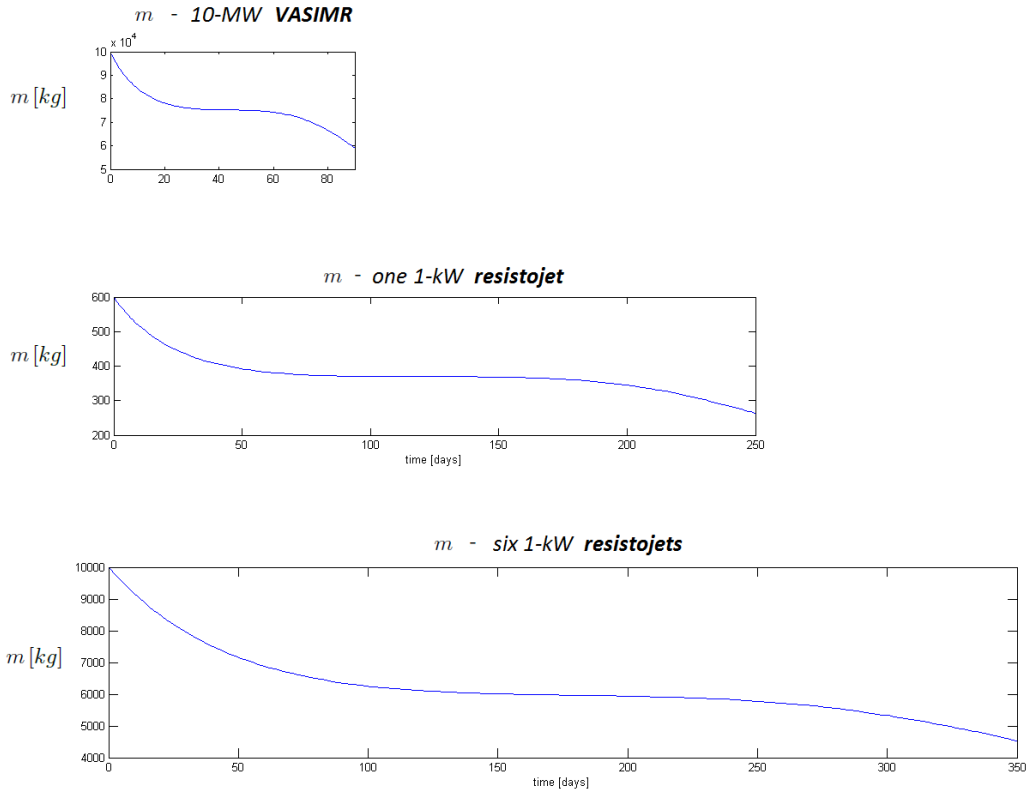

Figure 4.30: Mass trends in an Earth-to-Mars transfer obtained (from top to bottom) with the 10-MW VASIMR engine, the 1-kW resistojet used for the 250-*day* transfer, the six 1-kW resistojets used for the 350-*day* transfer.

Chapter 5

Conclusions

5.1 Validity of the Method

This work focused on the integration of different techniques in a unique, robust, algorithm capable of managing spiral dynamics in low-thrust motion.

The high non-linearity of this problem has been counteracted through the use of numerical techniques, such as *simple shooting* and *multiple shooting*.

Furthermore, test cases that relate the optimization both of the thrust acceleration (Case A) and of the propellant consumption (Case B) have been studied and the optimization process was performed through indirect methods. They can provide very accurate solutions (contrarily to direct methods) but require a very precise first guess solution. At this purpose, two main techniques were conceived: the *Adjoint Control Transformation* (ACT), described in Section 3.1.1, and the *Polar Curve Fit* (PCF), analyzed in Section 3.1.2.

As a result, the presented method demonstrated to be:

- *flexible*;
- *accurate*;
- *computationally efficient*.

5.1.1 Flexibility of the method

The method can be considered *flexible* as it succeeded in managing heterogeneous mission scenarios, such as an Eart escape, a LEO-to-LEO transfer, a LEO-to-GEO transfer, and a Mars-to-Earth transfer, which have been analyzed and solved (Chapter 4) with different kinds of optimization, as both

the accumulated thrust acceleration (Case A) and the propellant consumption (Case B) have been optimized. Moreover, mathematical passages have been derivated in Section 3.4 in order to quickly get a first guess solution of Case-B problem, once Case A is solved, by only inputing the initial mass m_0 of the spacecraft and the maximum power level P_{max} of the engine.

Different main attractors have been considered, as both test cases where the Earth and the Sun represented the main attractor have been analyzed. The implemented method succeeded to identify the solution in both scenarios, although the variables assumed values of very different orders of magnitude.

Finally, different propulsive performances have been managed, as engines with the typical performances of a resistojet ($P_{max} \approx 10^0$ kW) and of a futuristic nuclear-reactor engine, the "VASIMR" ($P_{max} \approx 10^1 \div 10^5$ kW), have been tested. Furthermore, the implemented method enabled the introduction of a control saturation (Section 3.4.1).

5.1.2 Accuracy of the method

The accuracy of the method addresses the capability of generating both good first guess solutions and optimal solutions.

As far as the first guess solutions are concerned, they are recovered thanks to the use of two conceived techniques: the *Adjoint Control Transformation* (ACT) and the *Polar Curve Fit* (PCF). The ACT allows to estimate the initial co-states by finding mathematical relations that link them to the thrust angles. The PCF exploits some regularities of the problem: if the position and the velocity variables refer to a polar coordinate frame and not to a classical Cartesian one, most of the co-states show a polar trend with respect to the fixed time of flight. With such technique it is possible to accurately estimate the initial co-states also for transfers with a high time of flight, which generally introduce more numerically difficulties.

Moreover, the optimal solutions can be considered intirinsically accurate as they are recovered through the use of an indirect method.

5.1.3 Computational efficiency

All the test cases presented in Chapter 4 have been run on a laptop, whose main characteristics are reported in Table 5.1.

As a result, the time elapsed in all the simulations is shown in Table 5.2, where:

Processor	i3-2350M
Clock speed	2.3 GHz
RAM	6 GB
Operating System	Windows 7

Table 5.1: Performances of the computer used for the implementation of the test cases

- *CASE A* refers to the problem analyzed in Section 2.1, that is the minimum-energy problem in which the cost function J_A penalyzes the accumulated thrust acceleration a:

$$J_A = \int_{t_0}^{t_f} [\frac{1}{2}a^2]\, dt \tag{5.1}$$

  - *Simple shooting* refers to the numerical technique explained in Chapter 3 and is represented by Steps 1 to 7 in the algortihm of Section 3.2 for the Case-A problem;
  - *Multiple shooting* refers to the numerical technique explained in Chapter 3 and is represented by Steps 8 to 10 in the algorithm of Section 3.2 for the Case-A problem;

- *CASE B* refers to the problem analyzed in Section 2.2, that is the minimum-propellant-consumption problem in which the cost function J_B penalyzes the final mass m_f of the spacecraft:

$$J_B = m_f \tag{5.2}$$

  - *Unconstrained* refers to the case in which no control saturation is imposed. The solution is obtained by following Steps 1 to 4 in the algortihm presented in Section 3.5 for the Case-B problem;
  - *Constrained* refers to the case in which a control saturation is imposed and whose implementation has been described in Section 3.4.1. The solution is obtaiend by following Steps 5 to 10 in the algortihm presented in Section 3.5 for the Case-B problem.

	Earth escape (150 day)	LEO-LEO (3 day)	LEO-GEO (30 day)	Earth-Mars (350 day)
CASE A				
Simple shooting (Steps 1-7)	27.5 s	2.3 s	7.3 s	0.7 s
Multiple shooting (Steps 8-10)	28.1 s	0.7 s	9.0 s	0.5 s
CASE B				
Unconstrained (Steps 1-4)	not tested	0.4 s	1.2 s	0.3 s
Constrained (Steps 5-10)	not tested	1.2 s	11.3 s	1.2 s

Table 5.2: Simulation time elapsed to solve the test cases. The Earth-Mars has been analyzed with three different times of flight (TOF), but only the case with $TOF = 350\ day$ is reported in the table, as the simulation time does not significantly change in comparison with the other two cases.

Observe that, despite the time of flight for the last Earth-Mars transfer is considerably high and equal to 350 day, its solution requires a low computational time due to the reduced number of trajectory revolutions. On the other hand, the Earth escape presents the higher simulation time because of the high number of trajectory revolutions.

5.2 Future Developments

The testing of a $200kW$ flight version of the VASIMR on the International Space Station in 2015 will be fundamental to determine the future steps to follow for the application of the VASIMR engines and consequently for the correct estimation of the mass and power budget to set in the implementation phase. The most crucial aspect, indeed, consists in evaluating if the results obtained by the optimization solver can be considered realistic or not. In other words, while the presented method is surely valid from a numerical point of view, future developements on the design and the integration of nuclear reactors are necessary to define the feasibility of the obtained results when a VASIMR engine is adopted.

Waiting for this to happen, a further step might consist in testing the presented mission scenarios not only with a variable Specific Impulse (VSI) model for the engine but also with a Constant Specific Impulse (CSI) one. This would allow the method to increase in *flexibility* as the test phase could be extended to many other kinds of thrusters.

A further step towards a higher flexibility of the method could also address the introduction of gravity assists during the transfer, which generally serve to save propellant by exploiting the gravitational attraction of massive bodies, such as planets.

As mentioned, once solved the minimum-thrust-acceleration problem (Case A), one only needs to input into the algorithm the initial mass m_0 of the spacecraft and the maximum power level of the engine P_{max} to solve the minimum-propellant-consumption problem (Case B). The value of P_{max} has always treated as constant but in reality it varies in time according to the current available power. Thus, a step forward can consist in elaborating a model for the engine capable of determining the time variation of P_{max} and, consequently, the maximum achievable thrust T_{max}.

Even if along the dissertation a complete 3-D formulation has been provided for all the conceived techniques, only planar-transfer test cases have been presented. The next step shall address test cases with a three-dimensional

dynamics.

Finally, a more accurate dynamical model shall be adopted in future studies, including the gravitational attraction of all major bodies in the Solar System as well as non-gravitational perturbations.

Bibliography

[1] Ho, D.Y., "The Year in Review: Electric Propulsion", *Aerospace America*, vol. 39, No. 12, 2001, p. 58.

[2] Ranieri, C. L., "Optimization of Roundtrip, Time-Constrained, Finite Burn Trajectories via an Indirect Method", *Journal of Guidance, Control and Dynamics*, Vol. 28, no. 2, March-April 2005.

[3] Lawden, D. F., "Optimal Trajectories for Space Navigation", *Butterworths*, London, 1963, pp. 79–94.

[4] Bryson, A. and Ho, Y. C., "Applied Optimal Control: Optimization, Estimation and Control", *Hemisphere Publishing Corporation*, NY, 1975, pp. 90-128.

[5] Breakwell, J. V., and Rauch, H. E., "Optimum Guidance for a Low-Thrust Interplanetary Vehicle", *AIAA Journal*, Vol. 4, No. 4, 1966, pp. 693-704.

[6] Pontryagin, L. S., Boltyanskii, V. G., Gamkrelidze, R. V., and Mishchenko, E. F., "The Mathematical Theory of Optimal Process", *Wiley-Interscience Publishers*, New York, 1962.

[7] Petropolous, A. E., and Russell, R. P., "Low-Thrust Transfers Using Primer Vector Theory and a Second-Order Penalty Method", *AIAA/AAS Astrodynamics Specialist Conference and Exhibit*, Honolulu, 2008.

[8] Caillau, J. B., Bonnard, B., and Picot, G., "Geometric and numerical techniques in optimal control and three-body motion", *Communications in Information and Systems*, Vol. 10, No. 4, 2010, pp. 239-278.

[9] Peng, H., Zhao, J., Gao, Q., and Wu, Z., "Nonlinear optimal control of the continuous low-thrust transfer between Halo orbits", emphIEEE, 2010.

[10] Caillau, J. B., Daoud, B., and Gergaud, J., "Discrete and differential homotpy in circuar restricted three-body problem", *Discrete and Discontinuous Dynamical Systems*, 2011.

[11] Casalino, L., Colasurdo, G., "Optimization of Variable-Specific-Impulse Interplanetary Trajectories", *Journal of Guidance, Control and Dynamics*, Vol. 27, No. 4, July-August 2004.

[12] Vadali, S. R., Nah, R., and Braden, E., "Fuel-Optimal, Low-Thrust, Three-Dimensional Earth-Mars Trajectories", *Journal of Guidance, Control and Dynamics*, Vol. 26, No. 6, Nov-Dec. 2001, pp. 1100-1107.

[13] Ranieri, C. L., "Indirect Optimization of Interplanetary Trajectories Including Spiral Dynamics", *PhD Dissertation, The University of Texas at Austin*, 2007.

[14] Hull, D. G., "Optimal Control Theory for Applications", *Springer*, New York, 2003.

[15] Rasotto, M., "Optimal Low-Thrust Transfers in Two-Body and Three-Body Dynamics", *Master Thesis, Politecnico di Milano*, 2012.

[16] Dixon, L. C. W., and Biggs, M. C., "The Advantages of Adjoint-Control Transformations and when Determining Optimal Trajectories by Pontryagin's Maximum Principle", *Aeronautical Journal*, Mar. 1972, pp. 169-174.

[17] Kluever Craig A., and Pierson, Bion L., "Optimal Low-Thrust Earth-Moon Trajectories Using Nuclear Electric Propulsion", *Journal of Guidance, Control and Dynamics*, Vol. 20, No. 2, Mar-Apr. 1997, pp. 239-245.

[18] Di Lizia, P., "Robust Space Trajectory and Space System Design using Differential Algebra", *PhD Dissertation, Politecnico di Milano*, 2008.

[19] Morring, F., "Commercial Route", *Aviation Week and Space Technology, McGraw Hill*, 172 (6), pp. 20–23, 2010.

[20] Aftergood S. et al., "Nuclear Power in Space", *Scientific American*, June 1991.

[21] Chang-Diaz, F., "The VASIMR Rocket", *Scientific American*, (http://www.adastrarocket.com/SciAm2000.pdf), Vol. 283, no. 5, Nov. 2000, pp. 90-97.